TAMPEREEN TEKNILLINEN YLIOPISTO
TAMPERE UNIVERSITY OF TECHNOLOGY

OSSI VUORINEN

CHARGE CARRIER AGGLOMERATES IN AN ELECTROSTATIC SOOT SENSOR

Master of Science Thesis

Examiner: Prof. Jorma Keskinen
Examiner and topic approved by the Faculty Council of the Faculty of Natural Sciences
on 9.11.2016

ABSTRACT

OSSI VUORINEN: Charge carrier agglomerates in an electrostatic soot sensor
Tampere University of Technology
Master of Science Thesis, V+43 pages, 6 appendix pages
October 2017
Master's Degree Programme in Science and Engineering
Major: Advanced Engineering Physics
Examiner: Professor Jorma Keskinen
Supervisor: M. Sc. Antti Rostedt

Keywords: Aerosol, soot, agglomeration, charge

Recently there has been development of a new compact on-board sensor to measure particle mass concentration. This electrical sensor is very compact and simple, and it has a wide measurement range and a short response time. The signal received from the sensor correlates well with results received using other commercial particle mass sensors.

The operation principle of the sensor is not totally understood. The sensor collects soot particles using a strong electric field and the current is measured from the depositing soot particles. However, the electric current received from the sensor is approximately three orders of magnitude larger than the current available from the natural charge of the particles. This implies that there must be some kind of process inside the sensor that amplifies the electrical signal.

The main hypothesis for this is the electrically stimulated agglomeration. In this phenomenon the soot particles accumulating on the electrodes form dendritic structures due to the electric field inside the sensor. After these dendrites grow to a certain critical length, large fragments called charge carrier agglomerates detach and move into the other electrode. These large agglomerates carry a very large total charge, and thus cause a large current signal in the sensor.

In order to validate this hypothesis the properties of the large agglomerate particles have to be well known. To investigate these large agglomerates a sensor mimicking cell was designed and built. This mimic cell consists of three parallel electrodes that can all either be set to a certain electric potential or used to measure accumulating current with an electrometer. The cell was also designed in a way that samples from the fragments could be taken to an electron microscope for further examination.

In this thesis the operation principle of the sensor was replicated with the mimic cell and the charge carrier agglomerates were examined. The two main properties, particle diameter and charge number, were defined for the charge carrier agglomerates. It was also investigated if the primary collection field strength had any effect on this phenomenon.

TIIVISTELMÄ

OSSI VUORINEN: Varauksenkuljettaja-agglomeraatit sähköstaattisessa nokianturissa
Tampereen teknillinen yliopisto
Diplomityö, V+43 sivua, 6 liitesivua
Lokakuu 2017
Teknis-luonnontieteellisen diplomi-insinöörin tutkinto-ohjelma
Pääaine: Teknillinen fysiikka
Tarkastaja: Professori Jorma Keskinen
Ohjaaja: DI Antti Rostedt

Avainsanat: Aerosoli, noki, agglomeraatio, varaus

Viime aikoina on kehitetty uudentyyppinen nokianturi, joka mittaa massapitoisuutta ajoneuvon pakosarjasta. Tämä sähköinen anturi on hyvin kompakti ja yksinkertainen, ja sillä on laaja mittausalue ja lyhyt vasteaika. Anturista saatu signaali korreloi hyvin muilla kaupallisilla mittalaitteilla saatujen tulosten kanssa.

Anturin toimintaperiaate ei kuitenkaan ole vielä täysin selvä. Anturista saadun signaalin suuruus on noin kolme kertaluokkaa suurempi kuin mitä mitattavien hiukkasten kuljettama varaus on. Tämä vääjäämättä merkitsee sitä, että anturin sisällä tapahtuu jokin ilmiö, joka vahvistaa sähköistä signaalia.

Tärkein hypoteesi signaalin vahvistukseen on tällä hetkellä sähköstaattinen kenttäohjautuva yhdistyminen. Siinä nokihiukkaset kerääntyvät elektrodien pinnalle anturin sisällä olevan sähkökentän vuoksi ja muodostavat säiemäisiä rakenteita. Kun säikeiden koko ylittää tietyn kriittisen pituuden, suuria agglomeraattihiukkasia alkaa irrota ja ne siirtyvät toiselle elektrodille. Nämä suuret agglomeraatit kuljettavat mukanaan erittäin suuria kokonaisvarauksia, ja siten ne aiheuttavat suuren virtasignaalin anturissa.

Tämän ilmiön tutkimiseksi on suunniteltu ja rakennettu anturin sähköistä rakennetta matkiva kenno. Tämä kenno koostuu kolmesta rinnakkaisesta elektrodista, jotka voidaan kaikki joko asettaa tiettyyn sähköiseen potentiaaliin tai käytetään mittaamaan kertynyt sähkövirta elektrometrillä. Kenno on myös suunniteltu siten, että irronneita agglomeraatteja voidaan kerätä erilliselle näytealustalle ja viedä näytteet elektronimikroskoopille jatkotutkimuksiin.

Tässä työssä pyritään toistamaan edellä kuvattu ilmiö rakennetun elektrodikennon kanssa ja tutkimaan tarkemmin irronneita agglomeraattihiukkasia. Näille määritetään myös hiukkasläpimitta ja varausluku virtamittausten ja elektronimikroskopian avulla. Työssä tutkitaan myös alkuperäisen keräyskentän vaikutusta ilmiön tapahtumiseen ja irronneiden agglomeraattien rakenteeseen.

PREFACE

This Master's thesis has been done in the Aerosol physics laboratory at Tampere University of Technology. The work has been done as a project for EmiSense Technologies LLC, and I would like to thank this corporation for the funding of this thesis work. I'd like to thank Leta Woo from EmiSense for the discussion and comments related to the measurements of this work.

I would like to thank my examiner, professor Jorma Keskinen and my supervisor, M. Sc. Antti Rostedt for the opportunity to work in this project and for the support and guidance throughout this project. Many thanks also to the Physics Workshop, who created the cell mimic from Antti Rostedt's design and brought it to life. For all the great microscope images I'd like to thank D. Sc. Mari Honkanen, who always took the best possible pictures of my samples. I would also like to thank B. Sc. Paavo Heikkilä for tremendous help with collecting samples for this work. Overall, I want to thank all the co-workers in the Aerosol Physics lab for creating a nice and warm atmosphere to work in.

I would also like to thank all the people I have shared my time with. Thanks to Teekkarikuoro and Lempibändi for giving the joy of music all these years. And a big thank you goes to my family, who have kept me going all these years. Especially I want to thank my brothers Juuso and Janne for all the support. Last, but not least, I would like to thank Riikka for reminding me that there's more to life than just work.

Tampere, 23.10.2017

Ossi Vuorinen

CONTENTS

LIST OF SYMBOLS AND ABBREVIATIONS

Latin symbols

B	Mechanical mobility
C_c	Cunningham slip correction factor
D_f	Fractal dimension
d_{50}	Impactor cut-off diameter
d_b	Particle mobility diameter
d_c	Characteristic length for an obstacle
d_j	Jet diameter
d_p	Particle diameter
e	Natural charge ($1.602 \cdot 10^{-19}$ C)
EF	Enhancement factor for an electric field
E_L	Limit value for electric field on particle surface
F_d	Drag force in Stokes' law
g	Gravitational acceleration (9.81 m/s^2)
K_E	Coulomb law constant ($1/4\pi\varepsilon_0$)
n	Particle charge number
n_L	Charge number limit value
q	Particle charge
s	Stopping distance
Stk	Stokes number
Stk_{50}	Impactor cut-off Stokes number
V	Velocity between particle and fluid
v_0	Particle initial velocity
v_j	Flow velocity in jet
Z	Electrical mobility

Greek symbols

η_{eff}	Collection efficiency
ρ	Density
ρ_0	Density of water (1 g/cm^3)
ρ_{eff}	Particle effective density
ρ_p	Particle density
τ	Relaxation time
χ	Particle shape factor

Abbreviations

CCA	Charge Carrier Agglomerate
CMD	Count Median Diameter
CPC	Condensation Particle Counter
DMA	Differential Mobility Analyzer
DMPS	Differential Mobility Particle Sizer
DPF	Diesel Particulate Filter
ELPI	Electrical Low-Pressure Impactor
$PM_{2.5}$	Particulate Matter for particles smaller than 2.5 µm
SEM	Scanning Electron Microscope
SMPS	Scanning Mobility Particle Sizer

1. INTRODUCTION

Human activities cause a lot of fine particle emissions into the atmosphere. The largest anthropogenic particulate emission sources are transport, industry, power plants and household emissions (Karagulian et al., 2015). Particle emissions have been shown to have significant negative health effects (Lelieveld et al., 2015; Dockery et al., 1993). They have been shown to shorten the average lifespan of people, and in 2010 exposure to fine particulate matter estimated up to 3.2 million premature deaths (Straif et al., 2013). The threat is significant especially in large cities and densely populated areas. Globally about 25 % of $PM_{2.5}$-emissions in urban areas are caused by traffic (Karagulian et al., 2015). Some gaseous emissions are also emitted from traffic, for example CO_2, CO and NO_x emissions.

Emission limits are set to reduce these harmful emissions, which vary slightly according to country or continent. To meet these emission standards, vehicle manufacturers are obliged to improve the aftertreatment of gaseous and particulate emissions. Particulate matter from vehicle emissions has been reduced through a wide range of particle filters. In particular, diesel particulate filters (DPF) are widely developed (Guan et al., 2015), and also new innovations in the filters of the continuously investigated (Han et al., 2015).

To monitor the operation of these filters, sensors are needed to measure the particle concentrations. This way it can be ensured that the vehicle emissions stay within the national or continental limits. A common way to evaluate the amount of particulate emissions has been to measure the total particulate matter. Recently, a compact and cost-effective sensor has been developed called PMTrac® (EmiSense Technologies LLC). This sensor measures the total mass concentration of the particles directly in the exhaust gas. It consists of two coaxial cylinders, and an electric field is generated between them. Measurements made with the sensor correlate well with the results from other devices.

The sensor operating principle is not clearly understood. The operation of the sensor is based on the collection of the naturally charged soot particles, from which the charge is measured as an electric current. During the sensor operation it has been noted, that the measured current is several orders of magnitude higher, that what can be expected from the soot particle collection. One hypothesis based on dendrite formation in the high electric field and subsequent highly charged fragment detachment. These fragments would transfer their charge on the measuring electrode and amplify the received electric

current. Another hypothesis for the operation principle is based on electrostatic discharge from the dendrite structures but this is not investigated further in this work.

In a previous study a model has been constructed to describe the dendrite growth and fragmentation. The dendrite formation occurs using a two-electrode system and the natural charge of the soot particles generated in a combustion process. The dendrites are formed on the electrodes resulting in a quiescent period in the amplification phenomenon. The duration of this period is inversely proportional to soot concentration, and in normal operating conditions it can last hundreds of seconds. After the dendrites grow to a critical height, fragments start to detach from the dendrites. The detaching fragments were examined with optical methods. According to these measurements, the fragments are large, in the order of 10 μm, and they carry approximately tens or hundreds of charges. During this event the current on the measurement electrode rises rapidly to nanoamperes, which is likely due to the large charge of the detaching fragments. By this time the system has reached a dynamic equilibrium, where the dendrite formation and fragment detachment occur simultaneously with the same rate. (Bilby, et al., 2016)

This work studies the formation of these dendrite structures as well as the properties of the charge carrier agglomerate particles. First, a cell mimicking the sensor electrode system is built to observe the detatching charge carrier agglomerates in further detail. In this thesis the development of the cell structure is described in detail. The final mimic cell consists of three electrodes, each electrode can be set to an independent potential, or current measurement can be made from the electrodes individually. The proper functionality of this mimic cell is tested and an estimation of the collection efficiency is measured. After that the size distribution of the charge carrier agglomerate particles is studied using microscope images received from the scanning electron microscope. Using the size distribution and an electrometer measurement an average charge number is calculated.

2. SOOT PARTICLES: PROPERTIES AND PROCESSES

Soot is a pollutant often associated with vehicle emissions. It is generated mostly in diesel-powered engines, and the soot emissions in these vehicles are controlled with particular filters. Despite this the vehicle particular emissions are quite significant and they cause major problems in densely populated areas. Soot is known to have negative health effects, and it is a highly carcinogenic pollutant (Shiraiwa et al., 2012). Soot particles are especially dangerous due to their small size which enables them to travel deep into the respiratory tract, all the way to the alveoli (Broday & Rosenzweig, 2011). Vehicle particle emissions also contain some small concentrations of sulfuric acid and hydrocarbons.

In this section the main properties of soot particles are examined in further detail. The formation mechanism is presented in order to explain the irregular shape of the soot agglomerates. After that the relevant particle properties considering soot and this thesis work are introduced. Finally the electrical charging mechanisms of particles in general are examined and their importance in the case of soot particles is assessed. Also the conductive nature of carbon and the effect of this property on the behavior of soot particles is discussed as the charge and conductivity of soot is thought to play a major role in the phenomenon examined in this work.

2.1 Soot

Soot particles are generated as a result of incomplete combustion. They are generated especially in diesel engines due to their combustion mechanism, in which the combustion air and fuel are mixed in the combustion chamber. Soot is generated usually when the air-fuel ratio is low. A soot-producing flame can be easily identified by the characteristic yellow color.

Soot particles are formed when polycyclic aromatic hydrocarbons combine to each other. These are formed mainly of acetylene C_2H_2, which is produced under oxygen-deficient conditions. Initially acetylene C_2H_2 is combined with CH-molecules to form C_3H_3-molecules that combine with each other to form benzene rings C_6H_6. These benzene rings are combined with more acetylene or benzene molecules, and over time they grow to be the primary particles of soot agglomerates having a diameter of about 5 nm. A schematic diagram of the formation of primary particles is shown in figure 2.1.

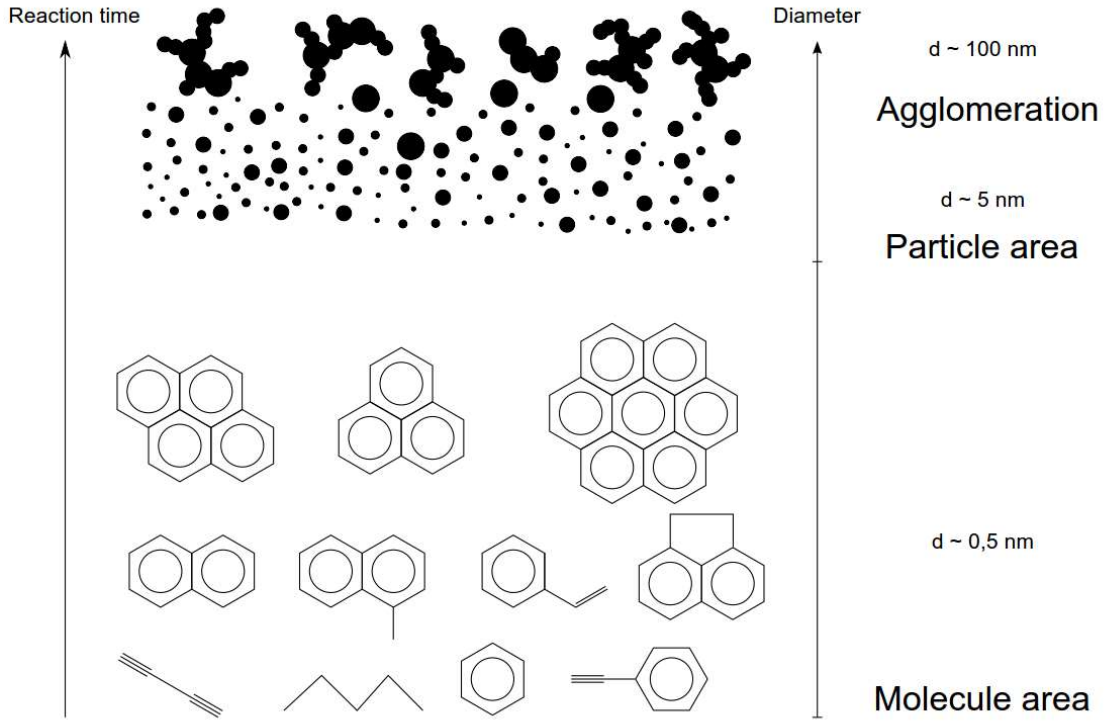

Figure 2.1 A visualization of soot particle formation in a combustion reaction. (Warnatz et al., 2010)

And so, the 5 nm primary soot particles are formed (Mathis et al., 2005). These are further linked with each other to form about 100 nm in size soot agglomerates whose fractal dimension is about 2.3 (Olfert et al., 2007). Soot particles consist mainly of carbon, and one soot agglomerate contains an average of 10^5–10^6 carbon atoms (Warnatz et al., 2010). Soot particles originated from diesel vehicles are bipolarly charged, and about 60–80 % of the particles are charged, and the rest of the particles are electrically neutral (Maricq, 2006).

The main requirement for the emergence of soot is a locally low amount of combustion air. In this case, a sufficient amount of acetylene is present in order to begin the formation process. Formation of the first benzene ring is a limiting factor in the reaction rate, as the growth and agglomeration take place quickly. Also, the temperature should be favorable, about 1300–2000 K. At lower temperatures, the amount of reactants is too low, and at higher temperatures the oxidation is rapid. (Warnatz et al., 2010)

2.2 Key properties of soot particles

These fine soot particles are called aerosol particles. Combined with the surrounding gas they form a colloidal system called an aerosol. The physics of aerosol particles is very unique since the particles are too large to be considered as molecules, but too small to be analyzed using basic mechanics. The size range of different aerosol particles is

very wide, ranging from 1 nm up to 100 µm. In the following section some basic aerosol particle properties regarding soot particles and the scope of this thesis are introduced.

2.2.1 Mobility

The main factors affecting an aerosol particle's movement in a fluid medium are the size of the particle and the fluid's ability to resist deformation or stress. As a particle is falling in a fluid, the particle experiences a drag force. When the flow on the particle surface is laminar, the drag force is received from Stokes' law as

$$F_{\mathrm{d}} = 3\pi\eta V d_{\mathrm{p}}, \tag{2.1}$$

where η is the fluid viscocity, V is the particle velocity relative to the fluid and d_p is the particle diameter. (Hinds, 1999)

As a continuum equation, the Stokes' law presumes that the velocity of the gas on the particle surface is zero. As the particle diameter approaches the free mean path of the gas molecules this presumption does not remain valid. To extend the applicability of Stokes' law to smaller particle sizes the slip correction factor C_{c} is used, which has an empiric formula of

$$C_{\mathrm{c}} = 1 + \frac{\lambda}{d_{\mathrm{p}}}\left[2.34 + 1.05e^{-0.39\frac{d_{\mathrm{p}}}{\lambda}}\right], \tag{2.2}$$

where λ is the mean free path, which is the average distance the gas molecules move between two consecutive collisions (Allen & Raabe, 1982).

The slip correction factor has notable significance, when the particle diameter is below 100 nm. When this is added to equation 2.1, the Stokes' law is corrected into form:

$$F_{\mathrm{d}} = \frac{3\pi\eta V d_{\mathrm{p}}}{C_{\mathrm{c}}} \tag{2.3}$$

The drag force makes it possible to get to measurable quantities. We can now determine the mechanical mobility B, which is the ratio of particle velocity and the exerting drag force:

$$B = \frac{V}{F_{\mathrm{d}}} = \frac{C_{\mathrm{c}}}{3\pi\eta d_{\mathrm{p}}} \tag{2.4}$$

In many electrical measuring instruments an electrical mobility Z is used, which is the product of particle charge and mechanical mobility:

$$Z = qB = neB = \frac{neC_c}{3\pi\eta d_p}, \tag{2.5}$$

where q is the particle charge, n is the particle charge number and e is the natural charge. Particle size is often defined from its mobility. However, in this case there is a possibility that larger particles with multiple charges have the same electrical mobility as smaller particles with a single charge. This causes some error when measuring particle size distributions with instruments measuring electrical mobility. This can be corrected if the charge distribution is well known. (Hinds, 1999)

2.2.2 Effective density

According to Newton's first law, a particle maintains its state of motion when the affecting total force is zero. When an aerosol particle is falling the velocity quickly becomes constant due to the gravitational force and the drag force being equal but in opposite directions. An equation can be formulated for the terminal settling velocity as

$$V_{TS} = \frac{\rho_p d_b^2 g C_c}{18\eta\chi} = \frac{\rho_0 d_a^2 g C_c}{18\eta}, \tag{2.6}$$

where g is gravitational acceleration,d_a is the particle aerodynamic diameter, d_b is the particle mobility diameter, ρ_p is the particle density, ρ_0 is the density of water (1 g/cm^3) and χ is the dynamic shape factor. When we combine the shape factor and particle density, we obtain an effective density ρ_{eff}, as in the following equation:

$$\rho_{eff} = \frac{\rho_0 C_c(d_a) d_a^2}{C_c(d_b) d_b^2} \tag{2.7}$$

The effective density contains information about the non-spherical shape of the particle. (Hinds, 1999)

With spherical particles the effective density is the same as the material's bulk density. A mass fractal dimension D_f can be defined for particles with a fractal-like structure (Virtanen et al., 2003). Effective density and fractal dimension can be combined using equation (Hinds, 1999)

$$\rho_{eff} \propto d_p^{D_f-3}. \tag{2.8}$$

D_f receives values between 1–3, where 1 is completely 1-dimensional (line), 2 completely 2-dimensional (e.g. plane) and 3 completely 3-dimensional (e.g. sphere) particle. 1- and 2-dimensional chained particles are formed from single spherical primary particles. They collide due to diffusion or some other mechanism and merge

with one another (coagulation) or stick to each other without merging (agglomerate). Especially in combustion processes agglomeration is fairly common.

Soot particles are an example of these combustion generated agglomerate particles with a fractal dimension smaller than three. Because of the soot formation mechanism these agglomerates are hard to break up to primary particles. Some information on the soot particle shape can be obtained by measuring the aerodynamic and mobility size distributions, and use that information to calculate the effective density.

2.2.3 Particle charging mechanisms

Soot, and all aerosol particles in general, have a significant probability to have an electric charge. This charge is caused by positive or negative ions attaching on the surface of the particle through different mechanisms. The charge distribution of a particle group is determined by charging process, and the charging probability is generally a function of particle diameter. There are primarily three possible particle charging mechanisms, which will be introduced next.

Thermal ionization is the main charging method in the case of soot particles (Balthasar et al., 2002). At high temperatures, for example in a flame, the surrounding gas molecules are ionized resulting into positive and negative ions (Hinds, 1999). These ions then attach on the surface of the soot particles. The bipolar charge distribution constructed through this mechanism is usually symmetric with respect to polarity (Hinds, 1999). In the case of soot particles studies have shown that around 60–80 % of the particles are electrically charged, half of the particles being positive and the other half negative, with a maximum of 4 elemental charges per particle (Maricq, 2006).

The ions in the air can also be generated in other ways. One option is to use a corona discharge where the particles are directed through an ion cloud generated by the corona. These ions then attach on the particles producing a unipolar charge distribution. This method is utilized in a corona charger used in the measurements of this work. The other option to create ions is to use radioactive materials, for example krypton. These chargers generates a well-known bipolar equilibrium charge distribution. Conserning these methods there are two processes to generate the charge distribution. In the first process called diffusion charging the collisions between ions and particles are caused by the Brownian motion. The other process is called field charging where an external electric field is added to guide the ions on the particle surfaces. Diffusion charging is the dominating process in small particle sizes whereas field charging dominates in large particle sizes. (Hinds, 1999)

The charge state of particles can change when coming into contact with a surface. The impact may result in charge transfer, which is due to two things: contact charging and

the transition of particle charge to the surface. This can be described using the following equation (John, 1995):

$$Q_{\text{total}} = Q_{\text{contact}} + Q_{\text{transition}} \tag{2.9}$$

Contact charging (Q_{contact}) is due to material differences in the desire to maintain their own electrons (Horenstein, 2004). The transferred amount of charge is associated to the work function of the materials. However, the charge transfer is not very common between conductive materials as local charge differences level out due to the free electrons in the electron structure of the metal (Matsusaka et al., 2010).

The transition of particle charge ($Q_{\text{transition}}$) is a fraction of the original charge of the particle Q_0:

$$Q_{\text{transition}} = \beta Q_0 \tag{2.10}$$

In the case of conductive particles in contact with a conductive surface, such as soot on a metal plate, all of the particle charge is transferred onto to the surface, meaning β = 1. For dielectric particles only a part of the original particle charge, and β is dependent on the contact area between the particle and the surface. (John, 1995)

Due to the repulsion of like charges there is a maximum value for the electrical charge on a particle. When solid particles receive a very large charge, the electric field on the particle surface gets so large that it starts to spontaneously emit electrones. This limit value for the charge number is

$$n_{\text{L}} = \frac{d_{\text{p}} E_{\text{L}}}{4 K_{\text{E}} e}, \tag{2.11}$$

where E_{L} is the maximum electric field induced on the surface. For electrons the value is $9 \cdot 10^8$ V/m. Emitting a positive ion is much harder and requires a larger electric field. In this case the field limit value is $2.1 \cdot 10^{10}$ V/m. This equation can be used to evaluate the charge numbers obtained for the charge carrying agglomerates later in this work. When liquid particles receive a sufficiently large charge number, the repulsive forces inside the particle become larger than the surface tension holding the particle intact. In this case the charge number limit is called the Rayleigh limit which is affiliated with much lower charge levels compared to solid particles. (Hinds, 1999)

2.2.4 Particle conductivity

The electrical properties of the particles are also affected by the conductivity of the particle material. This is a physical property more familiar with bulk materials, but the concept can be extended to aerosol particles. In principle, the particles can be categorize into two types based on conductivity, which are conductive and dielectric.

The conductivity of the particle affects on the charge distribution inside the particle. If the particle is of conductive material, the electric charge on the particle is evenly distributed througout the particle. If the particle is dielectric, the particle charge is on a fixed position where the charged ion has collided with the particle. The size of an ion is approximately 0.1 nm, which is for example about three orders of magnitude smaller than the average soot particle.

Particle charge behavior during surface deposition is also determined by conductivity. When a conductive particle attaches on a conductive surface it donates its electric charge to the surface, as discussed in the previous section. The charges move so that the charge distribution of the combined particle-surface-system is relatively constant. If the surface is externally set to a certain electrical potential, the particle also settles to the same potential and the same charge density which is on the surface.

3. PMTrac®: NEW METHOD FOR SOOT MONITORING

Due to the negative health effects of soot the particle emissions of combustion should be minimized. A major soot emission source is traffic which is highly regulated concerning all of the emissions. To meet the particle emission regulations diesel engines are fitted with diesel particulate filters. However, the accumulating soot and time-related wearing affect on the collection efficiency of the filter. As emission regulations tighten constantly, more and more performance is required from these filters. Sensors are needed to ensure that the filter is functioning properly and the emission regulations are met.

In priciple, there are two different methods to monitor the diesel particulate filter. The first one is to evaluate the amount of soot accumulated inside the filter. While this gives a good estimate of the state of the filter, it doesn't offer any direct information on the soot concentrations. The other method is to measure the soot concentration directly from the exhaust. These sensors use the different particle properties described in the previous chapter. Usually the electrical mobility resulting from electrical charge of the soot is a property of interest when observing the particles.

3.1 Particle emission monitoring

There are different technologies that are used to detect particle concentrations. One common type of sensor is called a resistive sensor. This type of sensor usually consists of two comb-like electrodes that are mounted close to each other on an insulating platform (e.g. Malik et al., 2011). The soot accumulating on the sensor creates dendrite structures between the electrodes and changes the resistivity of the electrodes. This gives information of the level of accumulated soot inside the filter. Unlike the electrostatic sensor, the resistive sensor doesn't give any information of the incoming soot concentration in real time.

The condition of the particle filter can also be monitored by measuring the pressure difference over the filter (e.g. Ohyama et al., 2008). This is done using a piezo-resistive sensor element which can be used to determine the level of load to the filter. A differential pressure sensor isn't a particle sensor in a traditional sense, since it doesn't give any direct information on the outcoming emissions. However it can be used to observe particle filter malfunctioning and the accumulated mass inside the filter.

Another method to evaluate the condition of the filter is using electromagnetic waves. This system consists of a particle filter integrated with an RF-transmitter and a receiver. The accumulated soot in the filter affects the propagating signal, and using this information the amount of soot inside the filter can be estimated. After further calculations an estimate of the spatial soot distribution inside the sensor can be obtained. These types of sensors have been developed in the radiowave frequencies (e.g. Sappok et al., 2016; Dietrich et al., 2015).

The particle concentration can be measured directly with an electrostatic sensor. Here the emissions are directed into the sensor and soot is deposited on the electrode inside the sensor. This accumulating particle mass creates a current on the electrode, which can be measured with an electrometer. The current reading can be calibrated to match a certain concentration, and thus it can be observed if the particle concentration is excessively high. The PMTrac® sensor (EmiSense Technologies LLC; Steppan et al., 2011) is an example of an electrostatic sensor and this will be discussed next in further detail. There are also other methods to measure the particle concentration electrically, for example measuring the current exiting the charger as is done in PPS-M (Pegasor Oy (Ltd); Ntziachristos et al., 2011)

3.2 PMTrac®

This electrostatic sensor measures electrically the concentration of the emission particles directly from the exhaust of a vehicle. The sensor is mounted to the exhaust line so that the measured exhaust flows by the sensor head at high velocity. The sensor

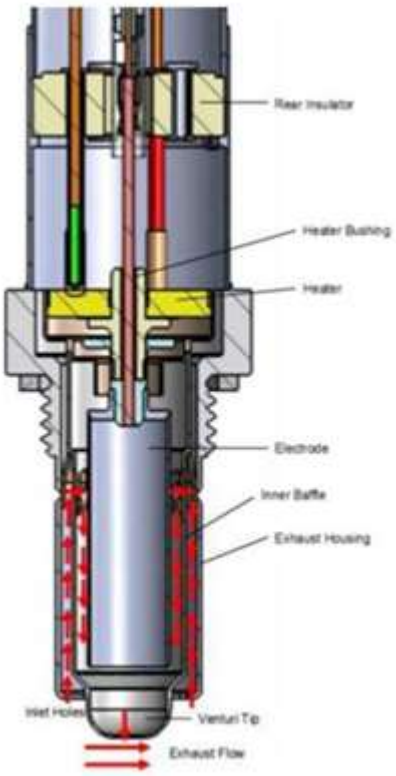

Figure 3.1 An illustration of the PMTrac® sensor (Bilby et al., 2016)

head is shaped so that the pressure difference caused by the flow forces a small part of the flow to flow through the sensor. This sample flow is directed between two electrodes, which are at different electric potentials causing a high electric field to the sample volume. The charged soot particles in the sample flow are collected to the electrode surfaces and an electric current is measured from the electrodes. A cross-section of the sensor can be seen in figure 3.1.

The concentrations of soot are usually relatively high. Over time the soot accumulates inside the sensor and may lead to an operation failure especially in such a compact sensor design as the one described above. This may be caused by the soot disturbing the current measurement or the flow profile inside the sensor as soot accumulates on the electrodes.

However, the accumulation of soot seems to have an overall positive effect on the sensor operation. The sensor has been found to produce a current in the range of nanoamps, instead of picoamps predicted from the original charge state of soot (Bilby et al., 2016). The sensor operation includes a quiescent time in the beginning of a measurement with a clean sensor, which indicates that the soot accumulation on the electrodes plays a significant role in the operation principle of the sensor. After a certain time the signal reaches a steady-state value, which is probably due to a dynamic equilibrium of accumulating soot and soot exiting the sensor.

3.3 Electrically stimulated agglomeration

As many electrical aerosol measurement instruments, the sensor described above collects soot particles using an electric field. Thus it is obvious that the particulate matter accumulates inside the sensor. However, the electric field significantly affects the formation in which these soot particles arrange. In this section the mechanics of this particle arrangement process is investigated in further detail.

The sensor primarily consists of a positive high voltage electrode and a grounded electrode, and the flow is directed between these two electrodes. As the primary soot particles are bipolarly charged they accumulate on the electrodes somewhat symmetrically. For simplicity, let’s observe a negative soot particle inside the sensor. The particle is directed on the positive electrode due to the electric field. A small current is observed on the current meter as the charged particle attaches on the electrode. Because of the conductivity of soot, the particle releases its charge immediately and is highly charged to the same potential as the rest of the electrode (Riehle & Wadenpohl, 1996).

At first, the particles attach on the electrode more or less randomly. As more and more particles accumulate, the new incoming particles tend to build up on the existing particles. This is due to the fact that an existing particle cluster amplifies the electric

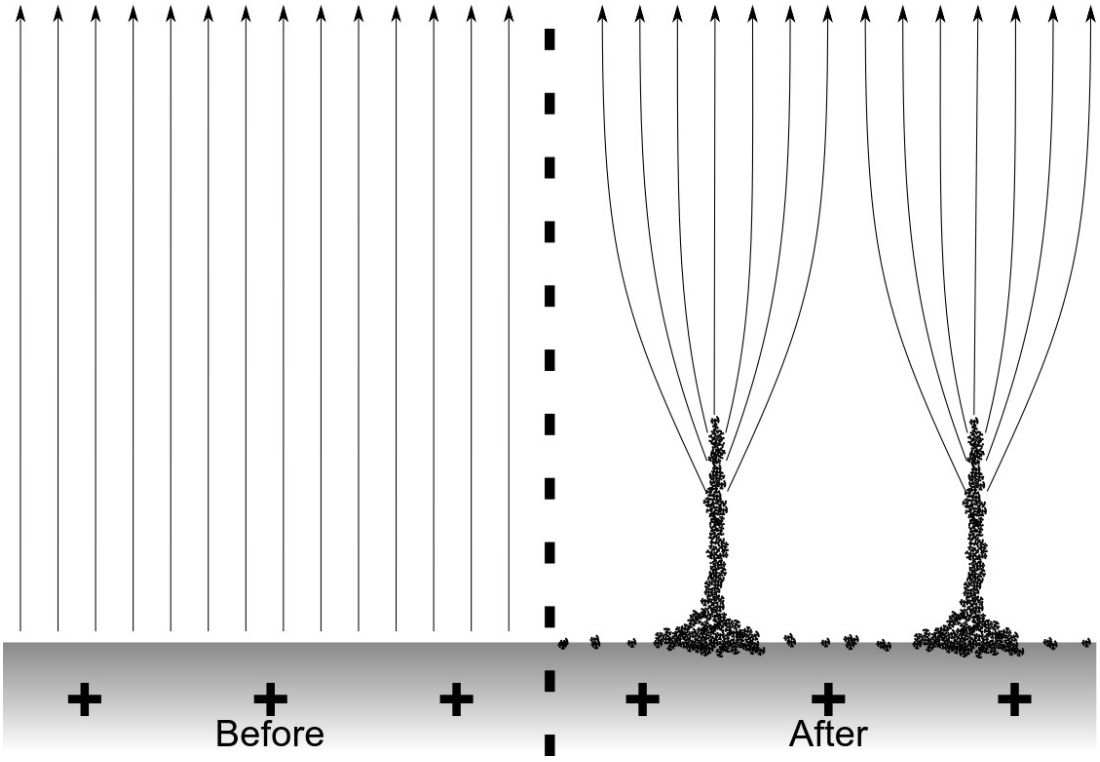

Figure 3.2 Conductive dendrite structures on the electrode cause a local disturbance in the electric field. Figure is not to scale.

field in the proximity of this cluster as it has a high positive charge. The phenomenon is demonstrated in figure 3.2. The field amplification has been tested using carbon nanotubes (Lu et al., 2007). This leads to really long and almost tree-like dendrite structures being generated on the electrode surface. This type of particle arranging is called electrically stimulated agglomeration which is typical for particles of low resistivity (Riehle & Wadenpohl, 1996).

The dendrite structures can grow really long and they have a very high charge. The length can be as long as 100 µm (Onischuk et al., 2003). Closer to the tip of the dendrite the adhesive van der Waals forces keeping the structure together are relatively weak, and the repulsive electrostatic force between the highly charged tip and the electrode is strong. At some critical length the repulsive electrostatic force exceeds the adhesive force which leads to a fragment of the dendrite to break off from the structure and return to the aerosol flow (Bilby et al., 2016). The detachment process is demonstrated in figure 3.3. The same agglomerate detachment phenomenon has also been studied using TiO_2-particles (Dalmaschio et al., 2012). The break-off always occurs in the interface of two primary soot particles as primary soot particles are very stable (Rothenbacher et al., 2008). In this work these fragments are referred to as charge carrier agglomerates (CCA) and they are the main target of interest.

As these CCA-particles start to detach from the dendrites the system builds up towards a dynamic equilibrium in a certain concentration. As more and more detachment occurs

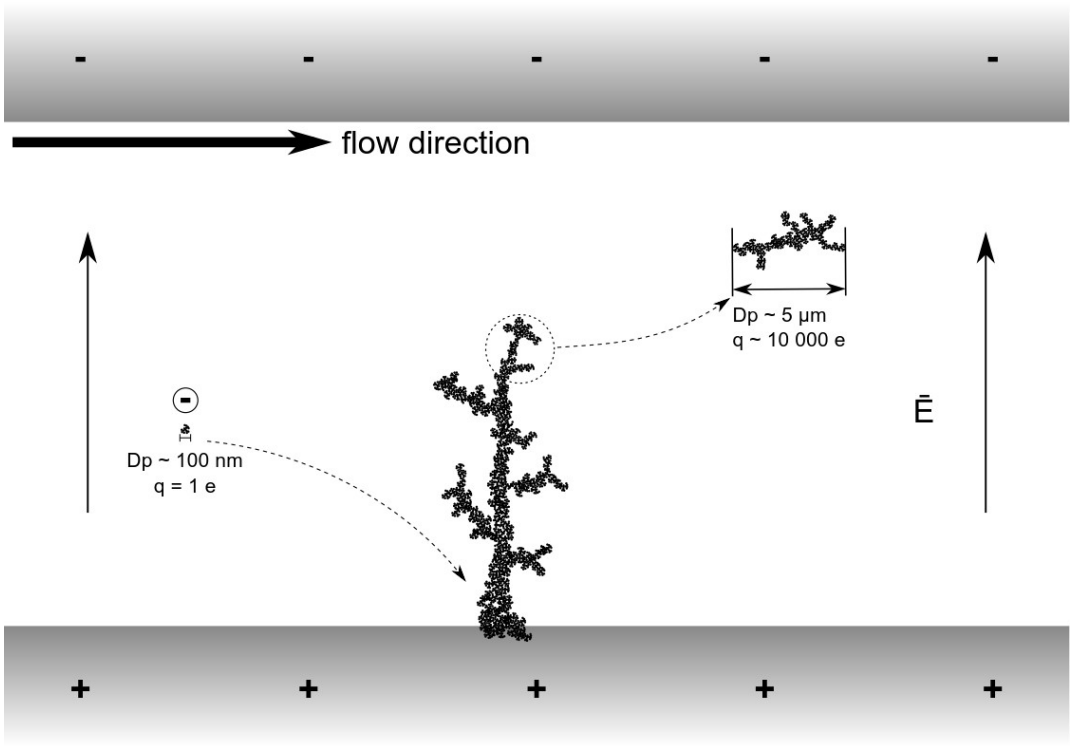

Figure 3.3 Soot particles attach to the electrode and break off after a certain critical length. Figure is not to scale.

the electric charge detaching rate also increases. After a certain time an equilibrium is reached and the amount of incoming soot from the particle emissions equals the outgoing soot due to the detaching CCA-particles. With a constant incoming soot concentration this would lead to a somewhat constant current on the collection electrode plate. However, if the incoming soot is increased the amount of detatching CCA-particles increases as well. A new equilibrium state is achieved and also the measured current due to CCA-particles increases. Respectively, if the incoming soot concentration is decreased the CCA-particle count and the measured current decreases. If the response of the measured current is well known with respect to the incoming soot concentration this enables to use that measured current to determine the soot concentration in different applications. (Bilby et al., 2016)

One effect that may enhance the current amplifications is multiple bounces of the CCA-particles. As the particles detach from the dendrites and impact on the opposite electrode they transfer their charge on that electrode. This may cause the CCA-particle to bounce from that electrode and return to the original electrode again obtaining a high charge number. The newly charged particle then returns to the opposite electrode and transfers its charge. This event may occur multiple times between the electrodes. When observing the charge of CCA-particles these multiple bounces interfere with the current measurements.

The CCA-particles are thought to induce the large current observed in the sensor. They carry a large charge as the dendrite they detach from is electrically a part of the high voltage electrode. It is presumed that these particles are significantly larger than primary soot particles but still have a similar fractal structure. The key factor in this phenomenon is the conductive nature of soot, so a better understanding could possibly benefit the measurement of other conductive particles. In the scope of this work the main interest is in the size, shape and charge of these CCA-particles.

4. DEVELOPMENT OF A SENSOR MIMIC CELL

The further investigation of the CCA-particles directly from the sensor would be extremely difficult. The large micron-sized particles deposit onto surfaces very easily and the large charge may also cause problems with traditional instruments. To better examine these large agglomerates a cell mimicking the electrode structure of the sensor was designed and built. The properties of most interest are the charge number and the diameter for the CCA-particles. Also microscopic image of these particles is essential in order to evaluate the composition and the shape of the agglomerates.

4.1 Concept of the mimic cell

The basic idea of the mimic cell is to obtain a similar structure compared to the sensor with a possibility of collecting samples. The electrode structure is similar to the sensor and the potentials and especially the electric field is set as close to the values used in the sensor. The flow velocity is set to a similar value as the sensor, though the larger dimensions of the cell will increase the volumetric flow rate. A collection plate is added in the cell to collect samples of the CCA-particles. The soot concentrations and the collection times are kept relatively small to minimize the case of multiple bounces described in the end of the previous section. Small concentrations also minimize the formation of dendrite structures onto the sample collection plate.

4.2 Methodology

The measurements in this thesis work were done at the in the Aerosol Physics Laboratory at Tampere University of Technology. The measurement instruments used and the soot generation system are introduced in the this section. Finally the constructed measurement setup is introduced.

Soot generation

Soot particle generation was done with a diesel-powered fuel heater (Webasto Air Top 2000 ST) shown in figure 4.1. With adjusting the stoichiometry of the heater's combustion process the soot concentration and the size distribution could be controlled. This is done by adjusting the fuel input and the air input to the combustion space. In a wide range measurement set with flow rates varying from 37 to 49 lpm, the particle size distribution obtained a geometric mean diameter of 27–164 nm, a geometric standard

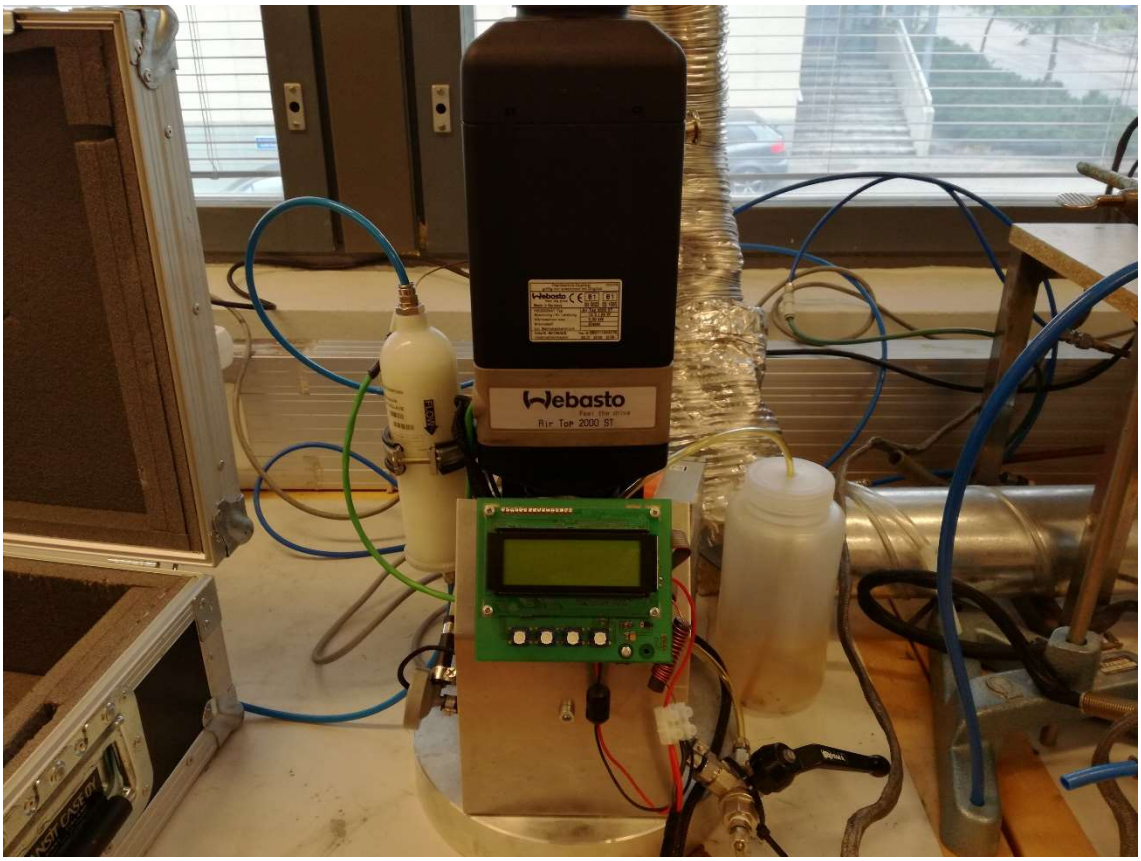

Figure 4.1 Diesel-powered fuel heater used to generate the soot used in the measurements.

deviation of 1.78–2.5 and a total number concentration of 1.94×10^6–4.52×10^8 #/cm^3. (Högström et al., 2012)

After the soot generator a virtual impactor is mounted to exclude any coarse micron-sized particles from the aerosol flow. The virtual impactor separates the particles using their inertia in a similar fashion as a regular impactor. (Solomon et al., 1983) First the aerosol is accelerated in the acceleration nozzle, after which 90 % of the original flow is sucked perpendicular to the original flow direction. The remaining 10 % continues through the impactor. Particles with a large mobility go through with the minor flow. Smaller particles on the other hand continue with the larger volumetric flow. This isn't actually a part of the soot generation system but for considering this work it was important to exclude the possibly re-entered coarse particles from the soot aerosol.

ELPI

The electrical low pressure impactor (ELPI) is a real-time measurement device of aerodynamic size distribution. ELPI combines a cascade impactor and an electrical measurement. First the particles are charged with a unipolar corona charger, where a high voltage corona wire creates ions. The charging method is mainly diffusion charging. After this the aerosol is directed through a cascade impactor, where there are 12 consecutive electrically measured impactor stages. The cut-off diameters are

between 30 nm–10 µm, and current is measured from every stage with an electrometer. In addition a vacuum pump is needed to create the low-pressure conditions and a measurement computer with the ELPI measurement software. (Keskinen et al., 1992)

SMPS

The particles can also be classified according to their electrical mobility. This property is applied with scanning mobility particle sizer (SMPS; Wang & Flagan, 1990). It practically consists of two different measurement instruments. First, a differential mobility analyzer (DMA; Knutson & Whitby, 1975) is used to select a specific particle mobility, and a condensation particle counter (CPC; Agarwal & Sem, 1982) is used to count the particles of that specific electrical mobility. When the DMA voltage is scanned through a certain area of electrical mobility, a mobility size distribution is obtained for the measured aerosol. Combining this information with an aerodynamic size distribution obtained with an ELPI, an estimate for the effective density of the particles can be calculated (Ristimäki et al., 2002). To improve the accuracy of the SMPS measurement, the DMA voltage can be increased incrementally and wait for the concentration to settle on each step. This instrument is called the differential mobility particle sizer (DMPS; Keady, et al., 1983).

Setup

The measurements were performed with a measurement setup as in figure 4.2. The soot particles are generated with the diesel-powered fuel heater, and this aerosol is transported into an air conditioning pipe and diluted with filtered compressed air. Next, the aerosol flows through a virtual impactor, which removes aerosol particles having a mobility diameter of more than 3 µm. After that the aerosol is passed through a corona charger, where the particles receive a negative unipolar charge. Then the charged particles go to the mimic cell in which particles are collected, depending on the

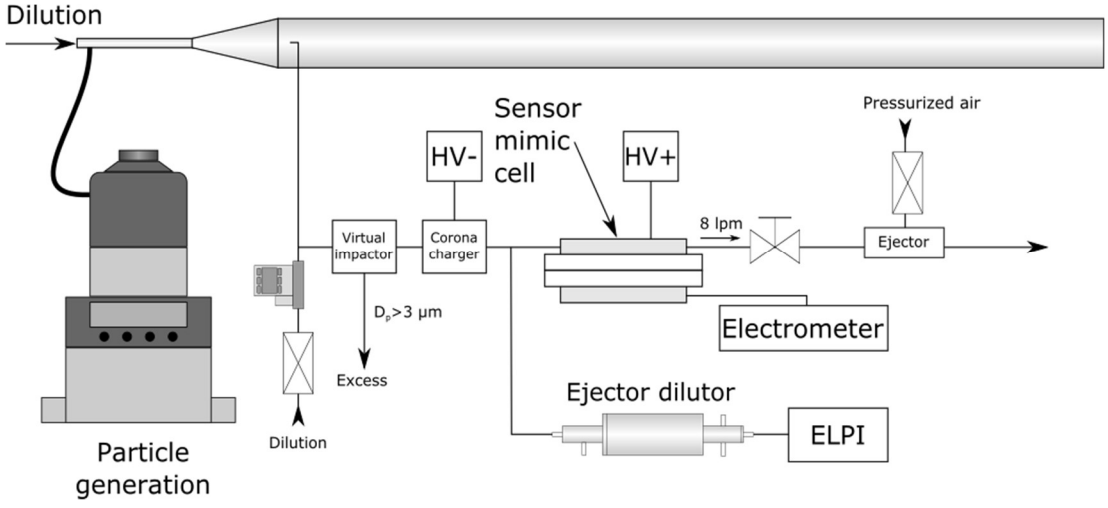

Figure 4.2 Measurement setup for the CCA-particle formation measurements.

measurement, either on the positively charged collection electrode or the measurement electrode. To assure a constant volumetric flow of 8 lpm inside the cell, suction is provided with an ejector. This volumetric flow corresponds to a velocity of under 1 m/s, which corresponds to the flow velocity inside the PMTrac®-sensor. At the same time the particle size distribution in the cell is monitored with an ELPI.

Microscope analysis

In electron microscopy an electron beam is directed on the sample. The electron source is usually a heated tungsten wire or single crystal tungsten, from which electrons are detached with a strong electric field. The released electrons are guided through several lenses to form a sharp beam which is directed onto the sample surface. The beam electrons scatter from the sample surface and simultaneously detach electrons or x-ray photons from the surface. (Kulkarni et al., 2011)

In this work a scanning electron microscope (SEM) was used to observe the generated charge carrier agglomerates. In this microscope the high energy electron beam is scanned across the micrographed sample area. A detector above the sample observes the detached secondary electrons. With SEM-microscopy up to 100,000-fold magnifications can be achieved, and the micrographs also deliver information about the morphology and topography of the sample. A SEM-sample has to be of conductive material, so that no electric charge is accumulated during the observation. (Kulkarni et al., 2011)

Microscopes in general offer good information on the size and shape of the particle. Most microscopes only offer two-dimensional images of the particles, so the shape of the particles is not perfeclty represented on the micrographs. There is no information of the particle shape in the third dimension, and the particles are not always regularly shaped, for example spheres. This particular problem can be seen in the case of soot particles, which are very irregular agglomerates. Although the microscope gives information on the particle shape, it is still difficult to present an unambigous particle diameter from micrographs.

There are two different diameters obtained from microscopic images which are used in the calculations of this work. The first diameter used is the Feret diameter. This is defined as a distance between two parallel tangential lines for a particle. It is sometimes called the caliper diameter, referring to measuring instrument. In this work, only the maximum Feret diameters are investigated, so therefore they are shortly referred to as Feret diameters. The other diameter used in this work is the projection equivalent diameter. This is defined as the diameter of a sphere that has the same projectional area as the observed particle.

4.3 Verification of the mimic cell concept

The operation of the mimic cell was designed to resemble the basic operation of the sensor. This can be summarized into two main components: significant amplification of the electric current and adequate collection of soot particles. Also concerning the hypothesis for the operation principle of the sensor it would be favorable to somehow detect the presence of CCA-particles and to observe their properties. The electrode structure in the mimic cell was designed to be easily adjustable and this property was utilized in these test measurements.

First, the current amplification phenomenon was observed in a measurement as a function of time during constant loading. In the beginning of a measurement the objective was to observe a small current which would increase approximately three orders of magnitude after a certain quiescent time. Next, the collection efficiency of the cell was defined in another measurement by alternating the polarity of the high voltage eletrode. After that a potential ramp measurement was executed to induce the detachment of CCA-particles from the dendrite structures.

4.3.1 Current enhancement

First the current amplification inside the cell was observed. The cell system used in this measurement can be seen in figure 4.3. A time-independent potential was set on the collection electrode of the cell, and also the electric field inside the cell remained constant over time. The electric field between the collection electrode and the

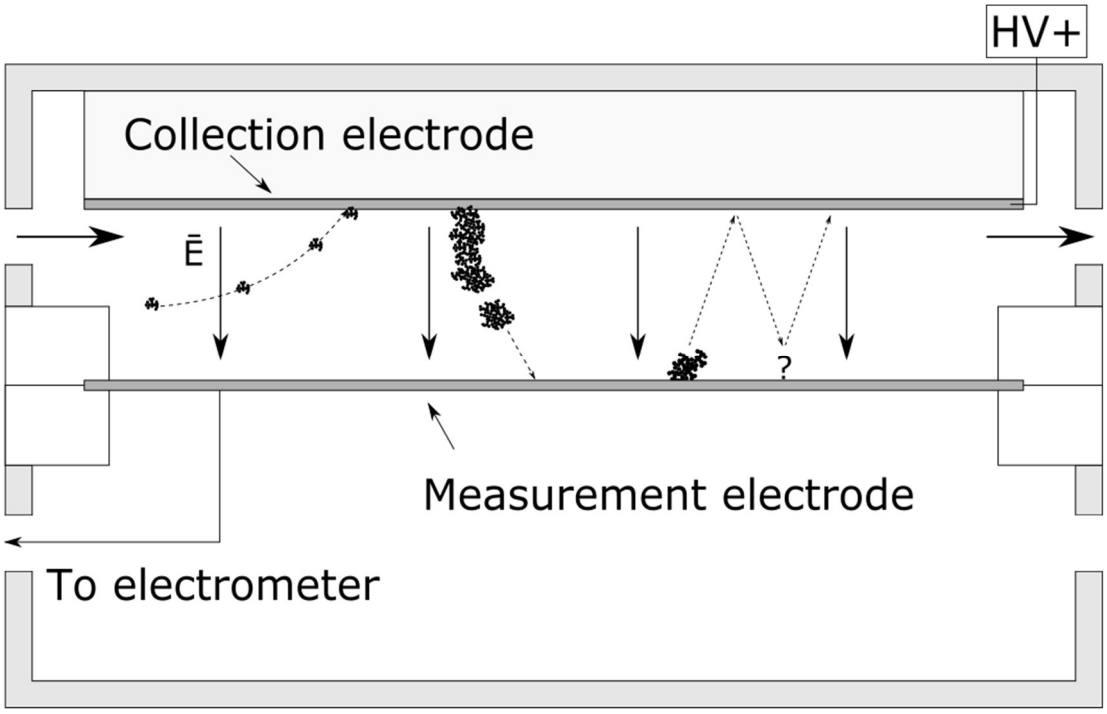

Figure 4.3 Visualization of the test cell in electrometer measurements.

measurement electrode was set to 500 V/mm. From the electrically floating measurement electrode the electric current was continuously measured with an electrometer. When the particles were introduced into the cell a small current could be detected in the measurement electrode. Over time the current increased presumably due to detaching CCA-particles from the collection electrode and thus amplifying the electric current. The ingoing particle population was also measured with ELPI, and with the received total current a current enhancement factor EF can be defined

$$\mathrm{EF} = \frac{I_{\mathrm{measured}}}{I_{\mathrm{incoming}}}, \tag{4.1}$$

where I_{measured} is the current measured with the electrometer and I_{incoming} is the current that comes into the mimic cell. This is calculated using the ELPI total current. When the volumetric flow rates through the cell and ELPI and the dilution ratio for ELPI is known, the incoming current can be calculated using equation

$$I_{\mathrm{incoming}} = \frac{\mathrm{DR}_{\mathrm{ELPI}} Q_{\mathrm{cell}}}{Q_{\mathrm{ELPI}}} I_{\mathrm{ELPI}}, \tag{4.2}$$

where I_{ELPI} is the total current measured by ELPI, Q_{cell} and Q_{ELPI} are the volumetric flow rates through the devices and $\mathrm{DR}_{\mathrm{ELPI}}$ is the dilution ratio before ELPI.

Electrometer current and the incoming current obtained from the current amplification measurement can be seen in figure 4.4. The blue solid line represents the current measured from the mimic cell electrode and the red dashed line represents the calculated incoming current using equation 4.2. The current takes a considerable amount of time to increase but a current enhancement effect can be observed. This

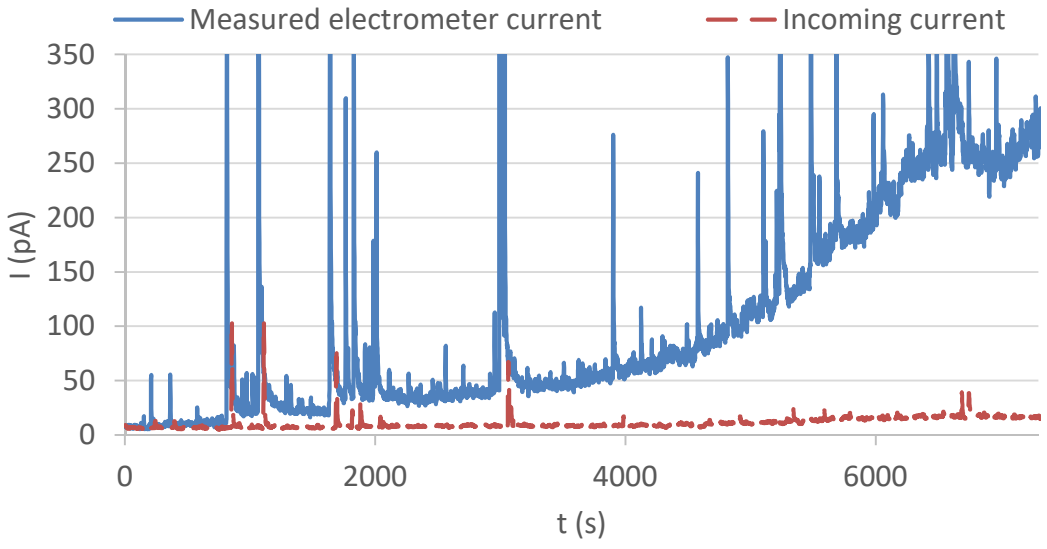

Figure 4.4 Electrometer current in a measurement as a function of time during continuous constant loading.

supports the hypothesis that soot dendrites are formed and large fragments detach inside the cell. The observed phenomenon corresponds fairly well with the signal development detected inside the sensor.

For this mimic cell geometry and collection field value a current enhancement factor can be calculated. Using equation 4.1 an enhancement factor of about EF = 15 is obtained. This value is much lower than what is observed in the sensor (EF ≈ 1,000). This may partly be due to the smaller collection field used in the mimic cell to prevent electric discharges. Also the larger dimensions may prolong the time to reach an sufficient amount of soot on the electrodes. This could cause the enhancement factor to increase in a much slower rate. However, it is found that the signal is significantly amplified and for this part the mimic operation resembles the sensor operation.

4.3.2 Particle collection efficiency

Next the functionality of the cell is tested with a small electric field. In this case, the current amplification should not be noticeable, and the cell should work as a electrostatic precipitator. The electric field between the collection electrode and the measurement electrode was set to 150 V/mm. The voltage source used was a bipolar voltage source, so the polarity of the collection electrode potential could be changed. The cell arrangement used in this measurement can be seen in figure 4.5. At first the collection electrode was set to a positive potential. Since the particles are negatively charged before the cell, all particles cling to the collection electrode and no current should be detected in the measurement electrode. After this, the polarity of the potential in the collection electrode is changed and the incoming soot particles cling to the

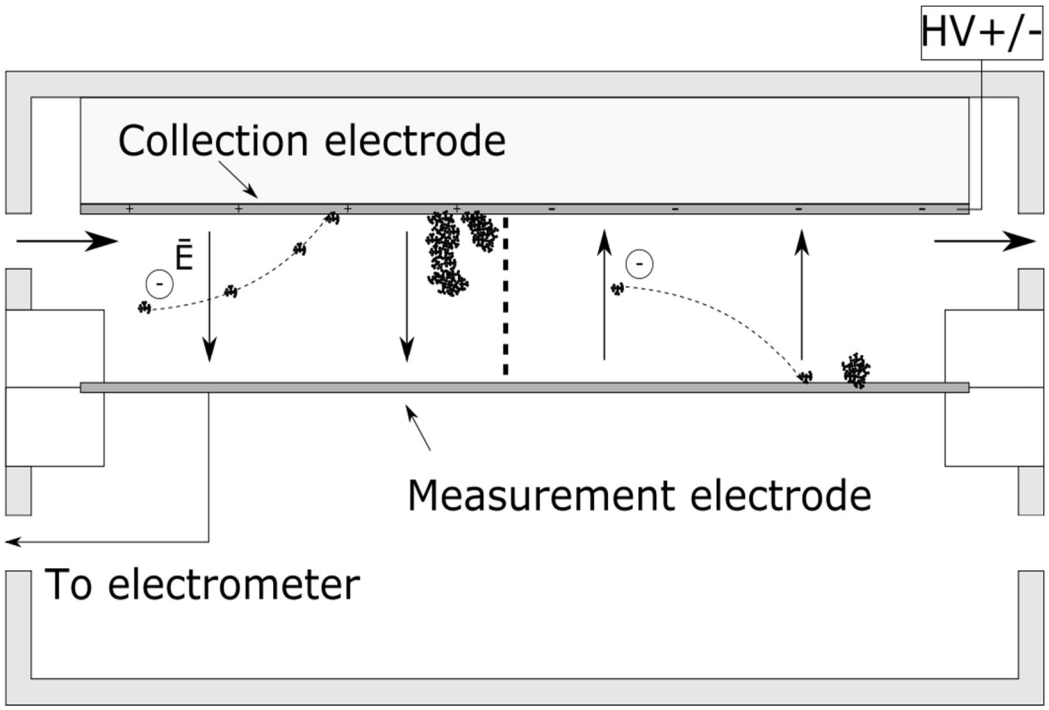

Figure 4.5 Visualization of the test cell in the collection efficiency measurements.

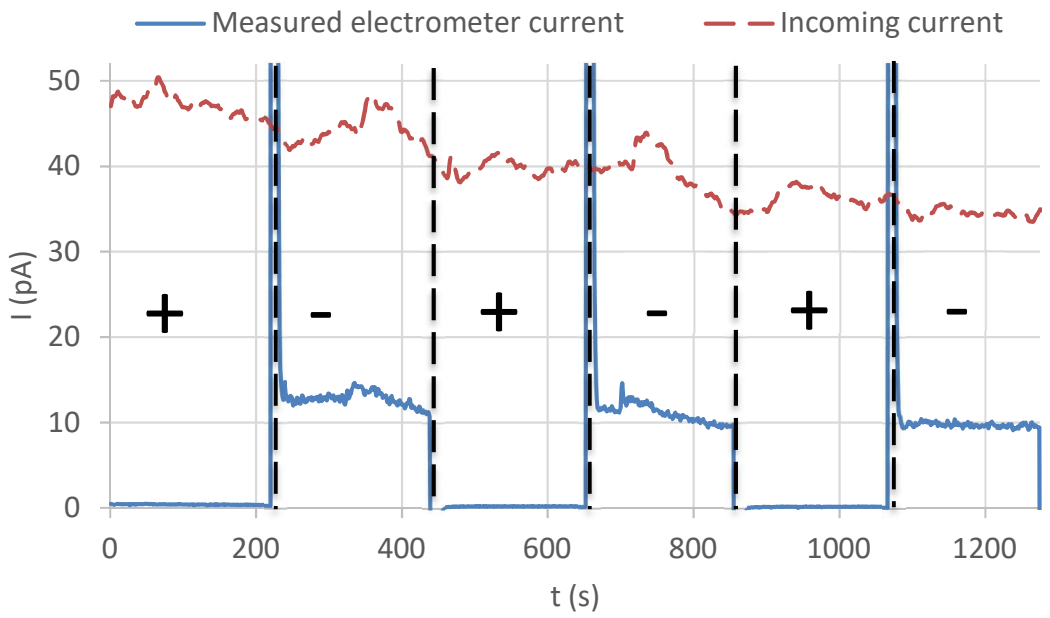

Figure 4.6 Electrometer current and incoming current using a low collection field.

measurement electrode inducing a signal on the electrometer. However, the electric field is so small that the amount of detachment from the dendrite structures on the collection electrode is relatively low which minimizes the formation of CCA-particles. Incoming particle distribution is constantly measured with ELPI as in the previous measurement. From the measured current and the ELPI total current a collection efficiency of η_{eff} can be calculated for the cell using equation

$$\eta_{\text{eff}} = \frac{I_{\text{measured}}}{I_{\text{incoming}}}, \tag{4.3}$$

which is very similar to the equation used for the enhancement factor earlier.

Results received from the low electric field bipolar measurement are shown in figure 4.6. With a positive collection electrode potential the signal always returns rapidly to zero, which is quite intuitive in the case of negative particles. When the collection efficiency is calculated using equation 4.3 and an arithmetical average is calculated over all three measurement periods, a collection efficiency of 28 % is received. This is quite low, but it can be assumed that with a higher collection field the collection efficiency should increase. However, in this measurement it had to be ensured that the formation of CCA-particles stayed minimal so the potential was kept low.

4.3.3 CCA-particle detection

After the operation of the mimic cell was verified to resemble the sensor operation, the next objective was to find the CCA-particles. The presence of these particles is the main element of the operation principle hypothesis so the first task was to create a

measurement that would verify this. This was done using a time-dependent linear potential ramp on the collection electrode after an adequate soot loading on this electrode.

The electric field required to detach the CCA-particles was defined using a linear potential ramp. When the collection electrode potential is changed linearly, it provides a constant current on the measurement electrode. This is caused by the increasing total charge on the collection electrode. These two electrodes have the same structure as a loading capacitor, which can be seen in figure 4.7 on the left. As the voltage is increased the charge decreases, which can be seen in equation

$$C = \frac{Q}{V} \tag{4.4}$$

The charge collecting on the collection electrode induces an equal, opposite-signed charge on the measurement electrode, and thus an electric current is observed. (Mansfield & O'Sullivan, 1998)

The change in the capacitor voltage can be derived from equation 4.4, and we receive the following equation:

$$\frac{dV}{dt} = \frac{d}{dt}\left(\frac{Q}{C}\right) = \frac{1}{C}\left(\frac{dQ}{dt}\right) = \frac{I}{C}. \tag{4.5}$$

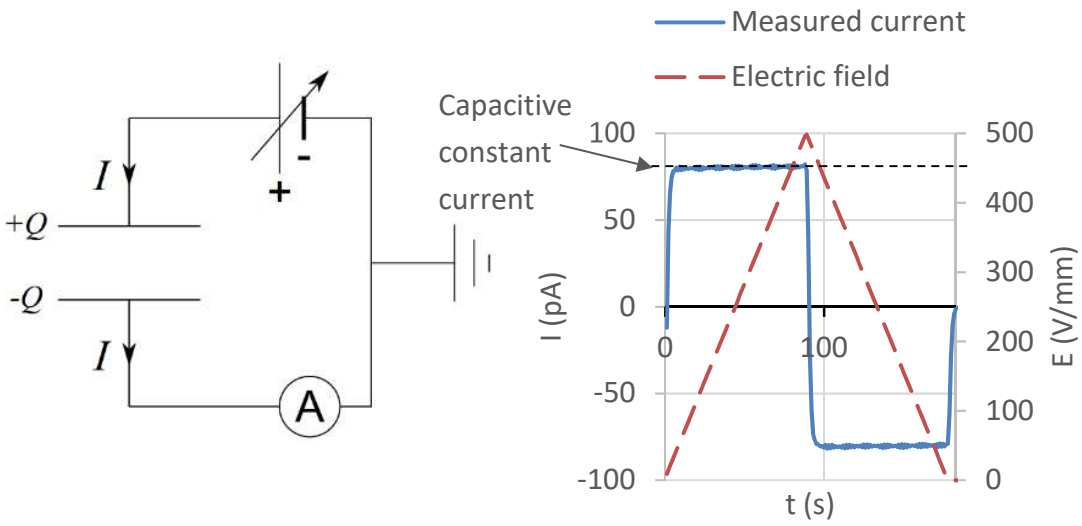

Figure 4.7 Induced current while loading a plate capacitor. When a high potential is connected on the collection electrode, it collects a positive charge. An electrostatic force induces an opposite charge on the lower electrode, which creates also a current on the lower electrode (left). If the potential is altered in a linear fashion a constant current is generated (right).

We can see that when the voltage increase rate is kept constant, the induced current in the capacitor is also constant. This constant current value is referred to as capacitive constant current, and a demonstration of this can be seen in figure 4.7 on the right. The capacitance of the capacitor is constant for it is dependent only on the geometry of the capacitor (Mansfield & O'Sullivan, 1998). If the measured current is greater than the capacitive constant current the additional current is presumed to be caused by the detaching CCA-particles due to the increasing electric field. This additional current is referred to as agglomerate current.

This phenomenon is used in the potential ramp measurements. The mimic cell configuration used in these measurements is similar to the earlier test measurements in figure 4.3. Before the actual measurements particles were collected to the collection electrode with a constant electric field of 150 V/mm for about one hour. This field value was chosen to minimize the current during the particle collection and to minimize the potential risk of CCA-particle detachment. After the collection the flow inside the cell was shut down and the potential ramp was executed. One ramp upwards lasted 90 seconds and during that time the electric field between the collection electrode and the measurement electrode was increased at a constant rate from 0 V/mm to 500 V/mm. The downwards ramp lasted also 90 seconds changing the field linearly from 500 V/mm to 0 V/mm. At the same time the induced electric current was continuously measured from the measurement electrode. As the electrometer current deviates from the constant current value it can be concluded that CCA-particles are coming off of the collection electrode and hitting the measurement electrode.

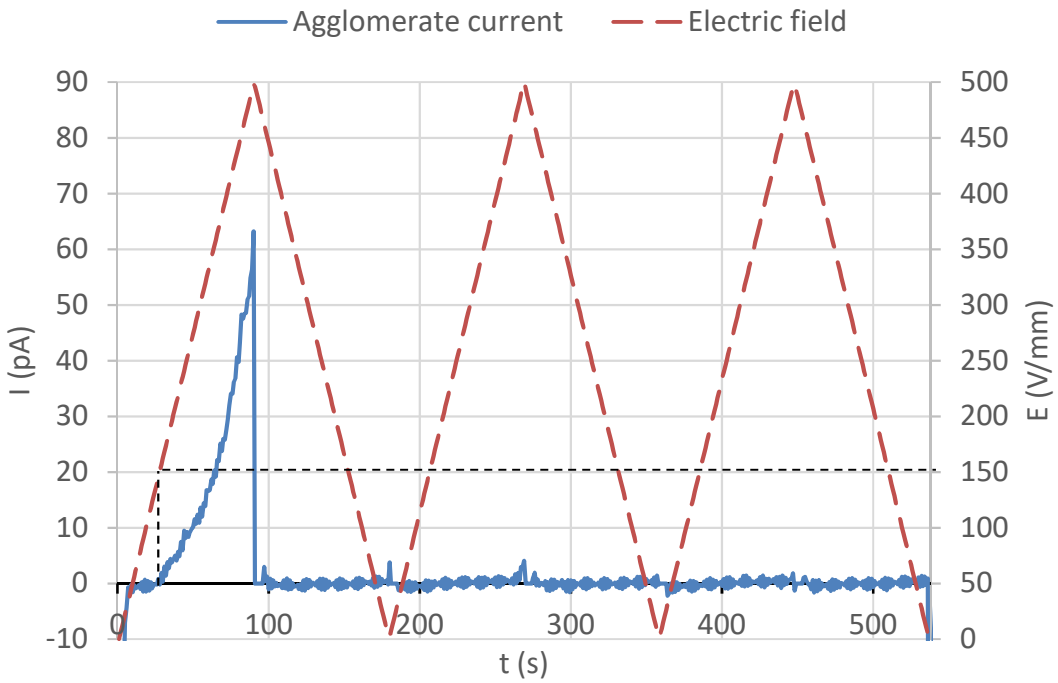

Figure 4.8 Agglomerate current versus the electric field in a potential ramp measurement.

The results received from the potential ramp measurements are shown in figure 4.8. The blue line is the agglomerate field described above and the red dashed line is the electric field inside the cell. The figure shows that after the field value exceeds 150 V/mm the agglomerate current increases significantly, and it can be assumed that this increase is due to CCA-particles detaching from the collection electrode. This field value is approximately the same as the collection field in this measurement, and after further measurements it was seen that the agglomerate current increases as the potential in the ramp reaches the collection field value. In the collection phase the field value may affect the structure and morphology of the dendrites and also the dendrite density on the electrode surface. However, this remains an open question and is not investigated further in this work.

The investigated phenomenon can't be characterized properly using the two-electrode system. The constructed measurement system is quite cumbersome as the collection times are very long and for this reason the amount of accumulated soot is very difficult to evaluate. There was some current detected during the collection period which may cause some unwanted additional particles onto the measurement electrode. The potential ramp seems to have some problematic issues. When the ramp changes direction at 500 V/mm it causes a significantly large disturbance to the electrometer distorting the current measurement. To evolve the CCA-particle collection and the current measurement a three-electrode system was developed which will be introduced next in further detail.

4.4 Three-electrode mimic cell

The three-electrode system is the next version with the objective to observe the CCA-particles. The mimic cell was modified further to improve the current measurement. The cell was fitted with a perforated grid electrode between the two electrodes as in figure 4.9. The grid was set to a relatively low potential (100 V) compared to the primary collection electrode. Therefore above the grid there is a large electric field to induce the dendrite formation, and below the grid the electric field is significantly lower. This was to ensure that no dendrite formation occurs on the measurement electrode. Also a large section of the grid around the sample area was covered with aluminium foil to reduce turbulent flows between the grid and the measurement electrode.

The new cell configuration was mounted with separate removable SEM-sample holder. This offered the ability to take multiple samples quickly. A hole was drilled on the existing measurement electrode to make room for the sample platform. The current measurement was divided into two sections: the other current was measured from the SEM-sample area and the other current was measured from the rest of the electrode plate. This was to improve the accuracy of the accumulated charge on the sample. The

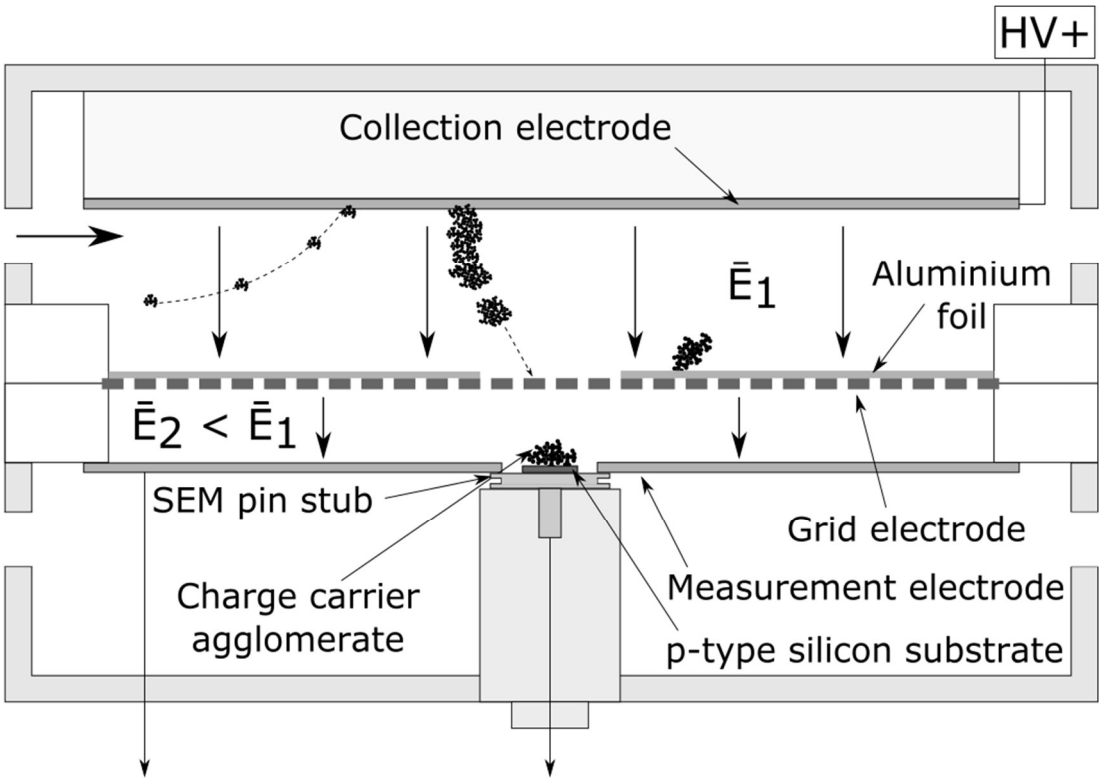

Figure 4.9 Visualization of the test cell using the three-electrode system

electrical isolation was done by attaching a thin layer of DuPont™ Kapton® polyimide film around the hole on the bottom of the measurement electrode.

The three-electrode system was developed to enhance the CCA-particle examination even further. The results from an example measurement are shown in figure 4.10. After introducing the aerosol into the mimic cell (small peak on the left), the current starts to increase, which could imply that the dendrite structures are forming and CCA-particles are detaching more and more. After approximately 150 seconds the current saturates to a certain value. This represents the dynamic equilibrium of accumulating soot on dendrites and detaching CCA-particles from dendrites. This leads to a constant CCA-particle accumulation rate on the measurement electrode causing a constant current.

Using the data in figure 4.10 an estimate of the efficiency of grid penetration is calculated. During the equilibrium phase the incoming current is approximately 75 pA. This value is multiplied with the enhancement factor calculated in Section 4 and the ratio of the SEM-stub area and the total grid electrode area to obtain a theoretical maximum current on the grid above the SEM-stub:

$$I_{\max} = I_{\text{incoming}} \cdot \text{EF} \cdot \frac{A_{\text{SEM}}}{A_{\text{electrode}}} \tag{4.6}$$

The diameter of the SEM-stub is 10 mm and the grid electrode area is approximately 90 mm × 10 mm. Using the EF value of 15 calculated in Section 4 a maximum current value of 98 pA is obtained. The average current measured on the SEM-stub in figure 4.10 is roughly 30 pA. Dividing this value with the theoretical maximum current the

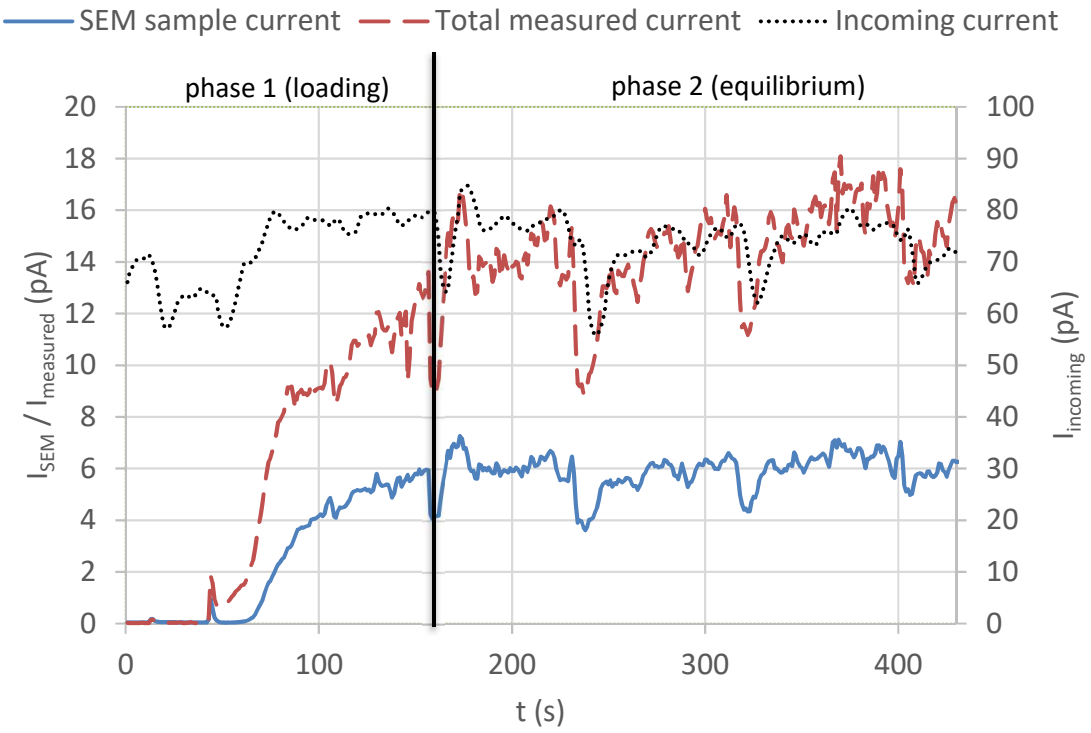

Figure 4.10 Current measurement in a three-electrode test. The electric field values were set to E_1 = 500 V/mm and E_2 = 29 V/mm as used in figure 4.9. The y-axis for incoming current is on the right and for other currents the left y-axis is applicable.

grid penetration efficiency is approximately 30 %. This value is further compared to the amount of holes in the grid. The ratio of holes to plate on the grid is approximately 50 % which makes the grid penetration efficiency extremely good. The obtained penetration efficiency may be overestimated because the enhancement factor might be even larger. This would result into a much smaller grid penetration. However, the amount of penetrating CCA-particles is fairly significant and the measurement system is likely to produce reasonably representative samples.

SEM-sample collection platform

Simultaneously with the current measurement a SEM-sample is collected on an SEM pin stub with a sample plate attached on it. This allows a relatively fast and easy method to gather samples at various collection conditions. As carbon is a conductive material, it is easy to take the samples directly from the measurement to SEM-analysis.

The sampling platform also has to be conductive and with a low surface roughness. The sample material was selected after analyzing several possible alternatives with SEM. The alternatives were p-type silicon substrate, polished steel, double-sided conductive carbon tape and TEM-grid used in transmission electron microscopes. After testing these materials it was found that the silicon substrate was the most convenient,

affordable and practical for these measurements and provided the good quality for the SEM-images.

The conductivity of the silicon was evaluated to ensure that it doesn't distort the electric field and interfere with the measurement. The resistivity of this silicon was estimated at 10–20 Ωcm. The thickness of the substrate used is approximately 350 µm and the surface area of the pieces is approximately 7 mm · 7 mm = 49 mm^2, so the maximum resistance would be (Mansfield & O'Sullivan, 1998)

$$R = \rho \frac{l}{A} = 200\ \Omega\text{mm} \cdot \frac{0.350\ \text{mm}}{49\ \text{mm}^2} \approx 1.4\ \Omega. \tag{4.7}$$

The electric currents in these measurements were of the order of 10 pA which would induce a voltage over the silicon substrate of

$$U = RI = 1.4\ \Omega \cdot 10\ \text{pA} = 14\ \text{pV}. \tag{4.8}$$

Compared to the grid potential of 100 V, this value is low enough by a large margin.

5. ANALYSIS OF CCA-PARTICLES

The three-electrode mimic cell configuration described above was used to observe the size and charge of the CCA-particles. These properties were defined combining two different components: the size distributions were calculated from SEM-images and the charge was calculated by combining that data with the current measurement. The measurement setup was the same as the one used in the test measurements (figure 4.2). ELPI was used to define the size distribution of the primary soot aerosol and the induced total current. The current induced by the CCA-particles inside the mimic cell was measured with an electrometer.

Before each measurement the mimic cell was opened and cleaned using a cloth and isopropanol to remove the excess soot from the cell. After that a small piece of double-sided conductive carbon tape was attached on the SEM pin stub also cleaned with a cloth and isopropanol. On top of this a small clean piece of silicon substrate was attached. After this the platform containing the SEM pin stub was screwed to the mimic cell and the electrometer cables and high voltage cable were connected on the mimic cell. The electrometers were left to be leveled for several minutes and then the electrometer zero level was measured.

Next the valves on both sides of the mimic cell were opened and the soot from the stabilized soot generator was directed through the mimic cell. The collection itself was done for a short period of time and the total accumulated charge was monitored to estimate the amount of accumulated material on the SEM pin stub. After a sufficient particle collection the flow through the cell was stopped with the valves. Finally the SEM pin stub was removed from the mimic cell and placed to a clean location to wait for SEM-analysis.

Before starting the measurements it had to be verified that the generated soot resembles vehicle particulate emissions. This was done by conducting a similar measurement containing SEM-sample collection and current measurement. In addition, a mobility size distribution of the primary soot was measured using SMPS before the mimic cell. Combining this with the aerodynamic size distribution obtained from the ELPI an estimate for the effective density could be calculated. These values were compared with results from earlier publications.

5.1 Data analysis

Combining the current measurement and the SEM-images to obtain the desired particle properties required some calculations. The total charge from the time integral of the measured current was quite straight-forward but to obtain the size distributions from SEM-images was more complex. To minimize the variance between images the same magnifications were used for all measurements. For the CCA-particles a 500x magnification was used, and for the primary soot particles a 25,000x was used.

5.1.1 Current measurement

The current due to the accumulating particles is measured from the measurement electrode below the grid electrode. Using the current measured from the SEM-sample stub, a numerical time integral is calculated to get the total accumulated charge onto the sample stub. The start and end point of the integral are defined directly from the moment the flow through the mimic cell was opened and closed, respectively.

5.1.2 SEM-sampling and -analysis

The sample was collected on the p-type silicon substrate that was attached on the SEM pin with double-sided conductive carbon tape. Multiple samples were taken with

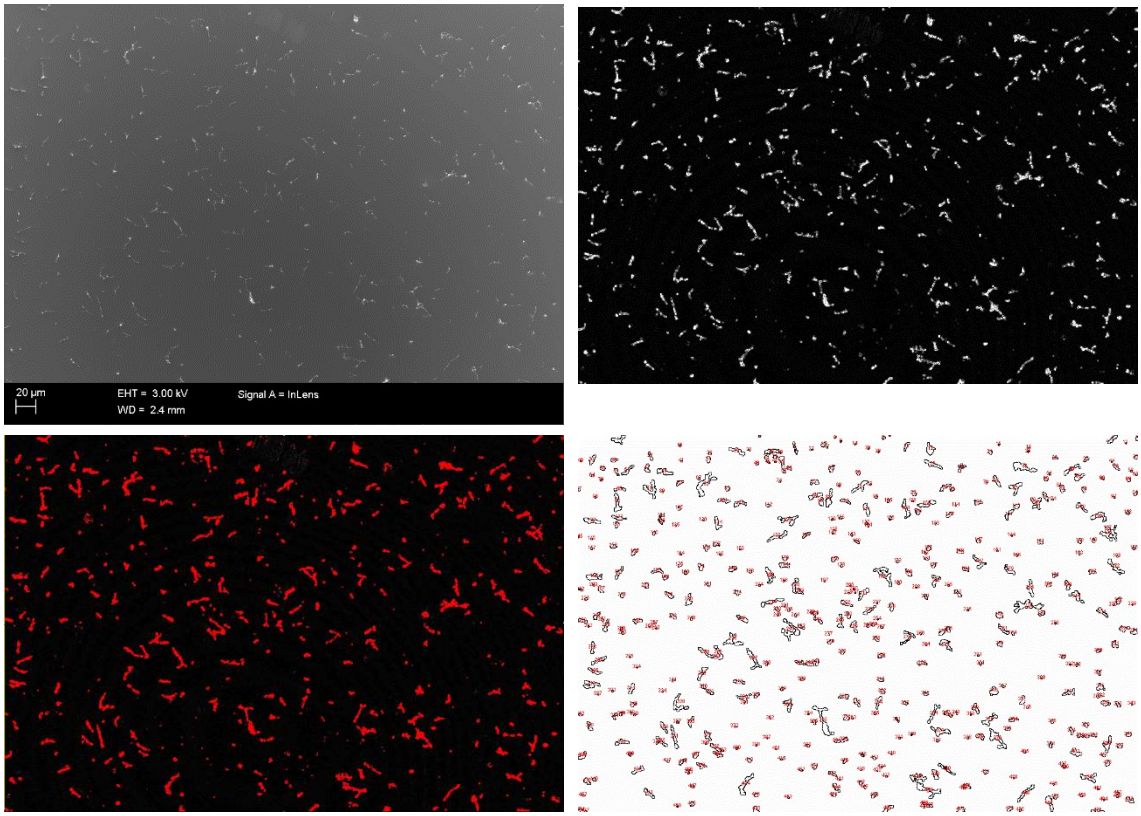

Figure 5.1 An example of the image analysis procedure using ImageJ-software.

different collection circumstances and they were analyzed with the SEM. The magnifications on the SEM-images were kept constant in all measurements to simplify the comparison between images from different measurements.

The obtained SEM-images were analyzed with the ImageJ-program (public domain, available at: http://imagej.nih.gov/ij). A certain analysis routine was done to minimize the error due to the variance in the image processing. The image analysis procedure is portrayed in figure 5.1. The original SEM-image is seen in the top left. First the image was enhanced using two processing tools in the program: sharpen and find edges. This way the edges of the particles are clearer and the diameters more accurate. Then a scale of µm/pixel is set to enable the program to determine true distances from the image. After this the scale is cropped from the picture to not interfere with the particle detection.

The enhanced image can be seen on the top right. For this image a threshold value for the particles is set, and the particles determined with this threshold are colored red (bottom left). This is the only step to include some visual estimation, since the threshold is selected so that all the particles seem to be covered. There might be some artefacts, and it may cause some error in the particle diameter values. After that the program is set to find the particles (bottom right) and define a projectional area and a Feret diameter for all of the particles. Two separate images are analyzed from every measurement and the data from these two images are combined.

5.1.3 Calculations

The main properties of interest on the CCA-particles were the charge number and the diameter. The particle diameter was obtained using the distributions from the analyzed SEM-images and by combining the distribution with the current measurement an average charge number was calculated. The size distributions were calculated using the projection equivalent diameter and the Feret diameter to estimate the fractal structure of the particles.

Since the particle size distributions are lognormal, the basic statistical key figures can be used to evaluate the distribution. The distributions were plotted using the particle diameter d_p on the x-axis and $dN/d\log d_\mathrm{p}$ on the y-axis where dN is the particle count in a certain diameter range and $d\log d_\mathrm{p}$ is the difference of the logarithms of the endpoints in that diameter range. The statistical figure calculated to represent the distribution was the count median diameter (CMD).

The average charge number was calculated using the particle projection area. The total eletrical charge accumulated on the collection electrode is denoted as q_tot:

$$q_{\text{tot}} = \int_{t_a}^{t_b} q(t)dt \tag{5.1}$$

This total charge is assumed to be evenly distributed on the electrode surface A_{tot} which is the area of the SEM-sample stub. The charge on one SEM-image is then calculated as

$$q_{\text{frame}} = \frac{A_{\text{frame}}}{A_{\text{tot}}} q_{\text{tot}}, \tag{5.2}$$

where A_{frame} is the area of one SEM-image. The calculations were done by combining two separate SEM-images so the charge on one frame is multiplied by two. Dividing this value with total particle count on both SEM-images N_{tot} and with the natural charge e, we obtain an average charge number for the collected particles:

$$n_{\text{avg}} = \frac{2q_{\text{frame}}}{N_{\text{tot}}e} \tag{5.3}$$

The size distributions were calculated from the information obtained using the ImageJ-software. The software calculates the Feret diameters for every particle directly but the projection equivalent diameter was calculated from the projection area provided by the software. This is done by calculating the diameter of a sphere that has the same 2D projection area as the measured particle.

The final results consist of the representative values for Feret diameter and projection equivalent diameter and also total particle count and average charge number for each measurement case. Every case contains two micrograph frames. The data of both images is combined and the median values for the Feret and projection equivalent diameter are selected as the representative values. The average charge number is calculated as described above using the total particle count. Finally, arithmetic mean values for all variables are calculated from all the measurement cases. Standard deviation values are also calculated to estimate the spread of the results in all of the cases (Pham, 2006).

5.2 Properties of generated soot

Before the CCA-particle measurements the primary soot from the soot generation system was examined. This was done to verify that the produced particles were similar to vehicle emission particles. An SMPS and ELPI distribution from the primary soot can be seen in figure 5.2. An approximation for the effective density was also calculated from this data. The density value was $\rho = 0.48$, which is quite close to values calculated in earlier research (e.g. Olfert et al., 2007). For this part, the generated soot particles seem representative for this purpose.

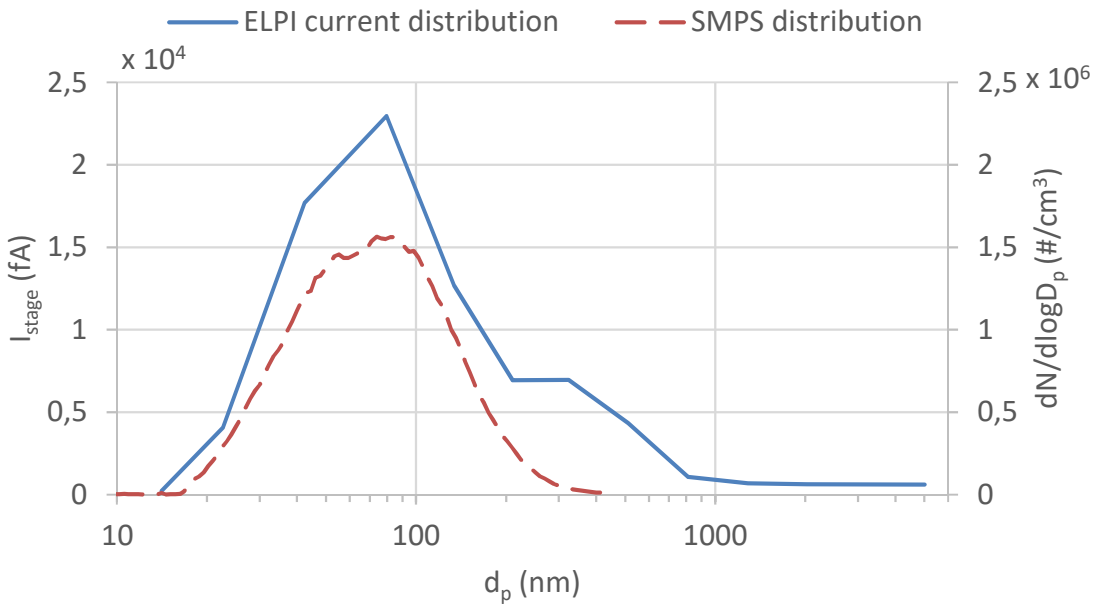

Figure 5.2 ELPI current distribution (solid) and SMPS distribution (dashed) of primary soot produced by the soot generation system.

For comparison, SEM-samples were also collected from the primary soot. The collection was executed with the three-electrode system in figure 4.9 with a few modifications. The perforated grid electrode was removed and the electric field was inverted so that the incoming soot particles accumulate directly on the measurement electrode. To prevent dendrite formation and detachment of CCA-particles a very low collection field (70 V/mm) and a short collection time were used.

An example micrograph can be seen in figure 5.3. Using this figure a size distribution can be calculated using ImageJ-software. From every micrograph two different size distributions are calculated. The other one is done using the Feret diameter and other one is the projection equivalent diameter. In addition, using the average projection area and the total electric charge accumulated on the electrode an average charge number for the particles is calculated.

The SEM-analysis provides an average Feret diameter of 92 nm and projection equivalent diameter of 69 nm. These values correspond quite well with values from the SMPS and ELPI measurements. The average charge number value is calculated to be 12, which seems rather high. Marjamäki et al. (2002) have calculated the penetration times average charge (Pn) for the ELPI corona charger used in this work to charge the primary soot. For a particle diameter of 80 nm the Pn number is approximately 3. The higher charge number received in these measurements may result from the accuracy of the measurement method on low electric charges. In spite of the low collection field the soot accumulation rate was very high and the collection times were very short (~20 seconds in figure 5.3). This makes it quite hard to estimate the level of soot accumulation and the soot particles are likely to overlap causing a seemingly larger charge per particle.

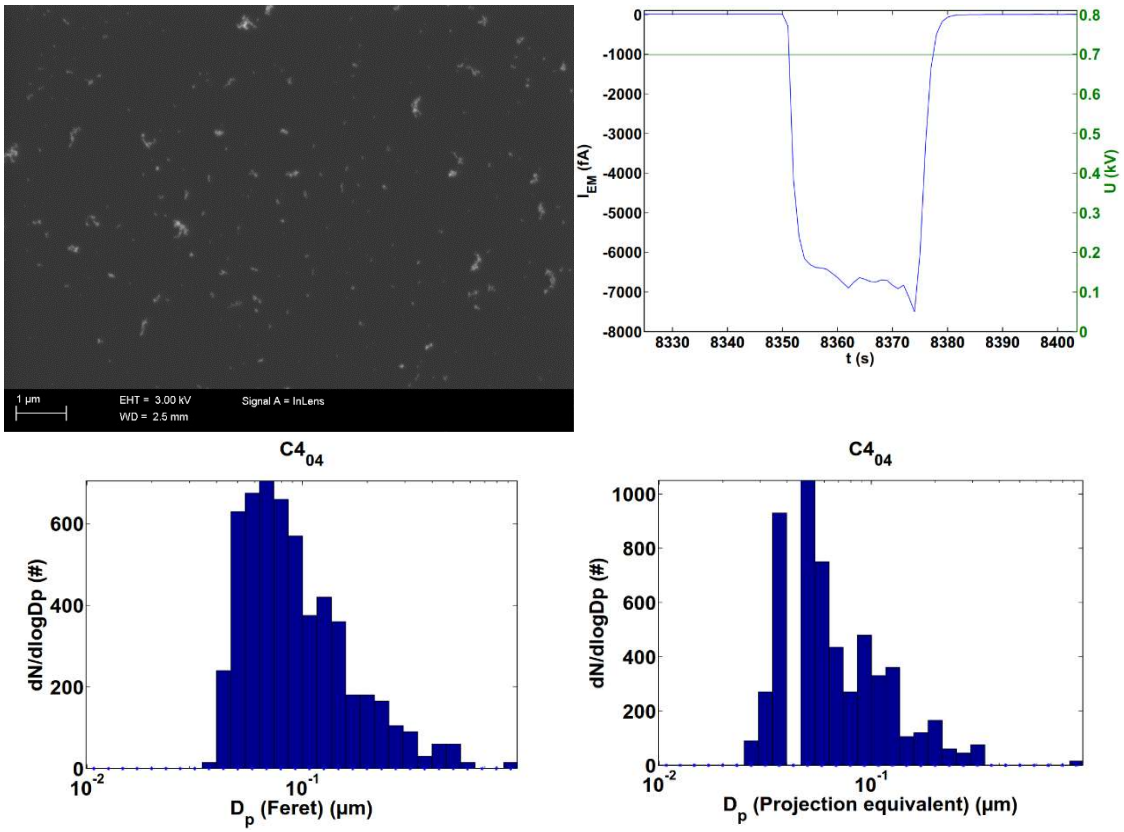

Figure 5.3 An example of the size distribution calculation done on one SEM-image in primary soot collection. Top left: SEM-micrograph from primary soot particles. Top right: current measurement from the particle collection period. Bottom left: Feret diameter number distribution. Bottom right: Projection equivalent number distribution.

Excessive soot accumulation seems to cause issues in the measurement. In samples where the total charge is larger the average charge number is increased significantly. In these samples there were also larger particles present in the micrographs. This could imply that there is dendrite formation present. As a sufficient amount of particles is collected on the electrode, the other incoming particles attach to them. This is due to the locally increased electric field in the proximity of the developing dendrite. It is possible that after a certain value the particle count visible on a single micrograph begins to saturate as the new incoming particles attach only on the existing dendrites and don't form new structures. The results all from the primary soot measurement cases can be seen in table A.1 in the appendix section.

5.3 CCA-particle properties

The CCA-particles were collected using the three-electrode system as in figure 4.9. An example micrograph can be seen in figure 5.4. The acquired SEM-images were analyzed in a similar fashion as in the previous section. Two different number distributions were calculated for each image using two particle diameters: the Feret diameter and the projection equivalent diameter. Using the total particle projection area, the average particle projection area and the accumulated electric charge we obtain an

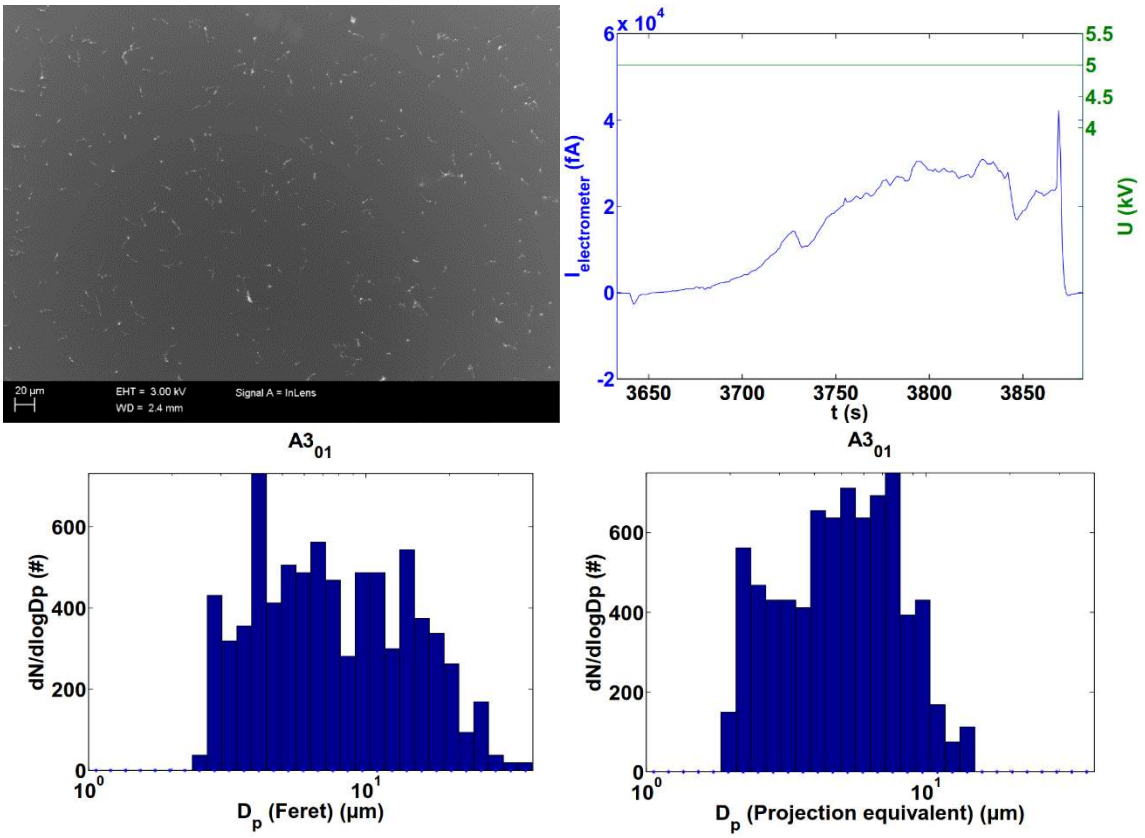

Figure 5.4 An example of the size distribution calculation done on one SEM-image in CCA-particle collection. Top left: SEM-micrograph from CCA-particles. Top right: current measurement from the particle collection period. Bottom left: Feret diameter number distribution. Bottom right: Projection equivalent number distribution.

estimate for the average charge number for a single particle. The results from all of the CCA-particle measurement cases can be seen in table A.2 in the appendix section.

The microscope images show that there is a distinct mode of large soot particles approximately 10 µm in diameter. Larger magnifications also shows some smaller particles in the range of 0.1–1 µm but not in significant amounts. The mode of large particles is also consistent with the distribution measured with the aerodynamic particle sizer (APS) at the electrostatic trap exit by Bilby et al. (2016). The microscope images from all of the measurement cases listed in appendix A can be seen in appendix B. In addition, the average accumulated charge per SEM-image determined from current measurements is listed below the images in that appendix section.

The calculated results can be seen in table 5.1. The top section of the table includes the average results for the primary soot analysis and the bottom section includes average results from the CCA-particle analysis with the addition of filtering the results based on particle count and collection field. The filtering was done to observe possible variation in the results. The error limits are defined from the standard deviation of the different measurement cases so it represents the statistical scattering of the measurements.

Table 5.1 Acquired properties for primary soot particles and CCA-agglomerates. (Error calculated as standard deviation of the results calculated from all cases.)

PRIMARY SOOT	**Cases**	E_{coll} **(V/mm)**	N **(#)**	d_{Feret} **(nm)**	d_{PE} **(nm)**	n_{avg}
All tests	5	70	650 ± 350	92 ± 8	69 ± 7	-12 ± 11
CCA-PARTICLES	**Cases**	E_{coll} **(V/mm)**	N **(#)**	d_{Feret} **(nm)**	d_{PE} **(nm)**	n_{avg}
All tests	9	100–500	590 ± 300	6.9 ± 2.8	4.7 ± 1.5	7200 ± 2300
Tests $N < 600$	6	200–500	420 ± 150	6.6 ± 3.2	4.4 ± 1.8	7600 ± 2100
Tests $E_{coll} = 500$	5	500	630 ± 380	6.6 ± 2.0	4.5 ± 1.4	6900 ± 1900

The large standard deviation values show that results calculated in this work are widely dispersed. This is partly due to the stochastic nature of the formation of CCA-particles (Bilby et al., 2016). It is also evident that smaller particle count seems to lead to smaller particle sizes which may result from fewer overlapping particles in the images. To reduce this bias in the results the total particle count per case is limited to 600 in the following further analysis.

Figure 5.5 shows the acquired projection equivalent particle size (left) and the average charge number (right) as the function of the collection field for measurement cases where the particle number per measurement case was below 600. The graph on the left shows no apparent relation between the collection field and particle size. On the other hand, the graph on the right shows a decreasing linear trend in average charge number with increasing collection field. The data is however quite scattered which can also be seen from the relatively low R^2-values, especially in the graph on the left.

The average CCA-particle diameters obtained from the cases in figure 5.5 were $d_{\mathrm{Feret}} = 6.6$ µm and $d_{\mathrm{PE}} = 4.4$ µm and the average charge number was $n_{\mathrm{avg}} = 7600$. The diameters are similar to the measurements done by Bilby et al. (2016) but the number of elementary charges per particle are almost two orders of magnitude higher in the results of this work. The collection fields used in measurements by Bilby et al. (2016) were 750 V/mm and 1250 V/mm. Extrapolating the trendline to that field range in the graph on the right of figure 5.5 the resulting charge numbers are approximately 0–4000. This coincides with the estimate of several tens or hundreds of charges done by Bilby et al. (2016).

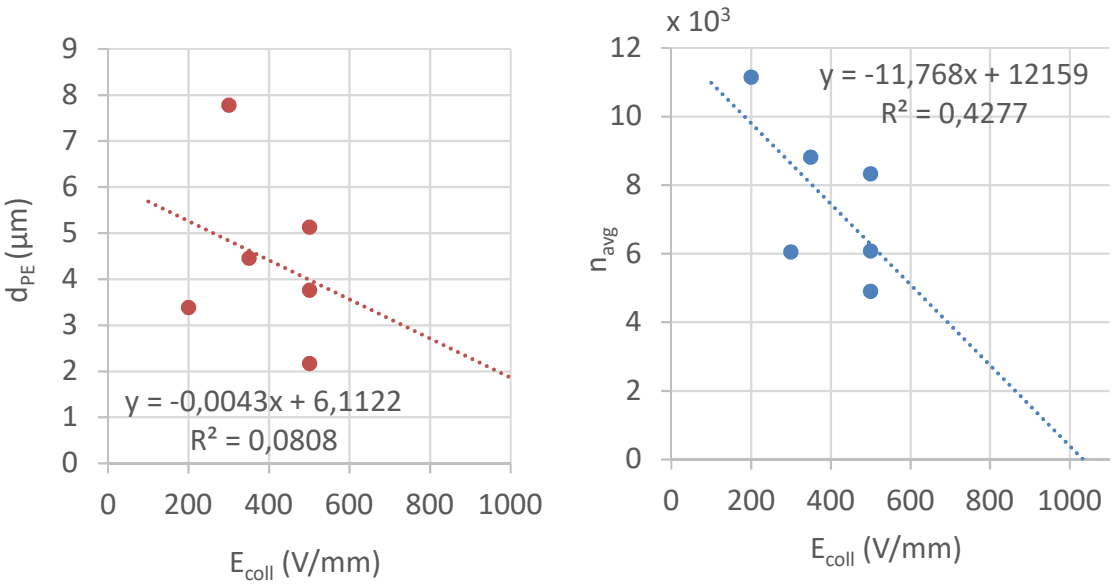

Figure 5.5 Projection equivalent size as a function of collection field (left) and the average charge number as a function of collection field (right).The data has been limited to a maximum particle count of 600 particles per measurement case.

However, there is a lot of uncertainty in the results calculated in this work. An significant problem noticed during the measurements is the repeatability of the results. This consists of both the stochastic nature of the phenomenon itself and the random error due to the measurement system used in this work. There were a lot of problems during the measurements concerning soot generation, flow control and the electronics of the mimic cell, for example electric discharges from the high voltage electrode. In spite of solving most of the problems there may be some improvements that could still be done to the measurement system.

The overlapping of particles in the SEM-images caused a significant bias in the results. As multiple particles stack on the measurement electrode it is seen on the SEM-image as a single particle which causes an increase on the average charge number in the results. The primary soot concentration was relatively high in the measurements which resulted into very short collection times and made it very difficult to avoid this excessive soot accumulation on the measurement electrode. The problem was emphasized on the primary soot analysis measurements.

6. SUMMARY

A commercial soot sensor produces a much larger signal than expected from theoretical predictions. A hypothesis to explain this very large current generated inside the sensor is examined and tested. The electric field inside the sensor collects the incoming soot particles from vehicle emissions, and these form dendrite structures on the high voltage electrode in the sensor. These dendrites receive a very large electric charge after which a part of the dendrite detaches and drifts on the measurement electrode.

To investigate this phenomenon an electrode cell mimicking the sensor electrode system was designed and constructed. In addition to the two perpendicular electrodes also a perforated grid was used between the electrodes to ensure that no dendrite formation occurs on the measurement electrode. The objective was to detect the current amplification and to investigate the properties of the detaching large agglomerate particles.

Based on the tests carried out in this project the sensor mimicking cell functions as a simplified sensor and amplifies the current signal. The collection efficiency of the mimic cell is relatively low at low electric fields. Still, the mimic cell can collect a sufficient amount of particulate matter for analysis. The observed delay time in current enhancement is several minutes, which would suggest that dendrite structures are formed gradually on the collecting electrode, and after a certain period of time the large agglomerate particles start to detach causing a current signal growth.

Signs from these large CCA-particles have been obtained in this work. Observing the acquired SEM-images, large approximately 5 µm soot agglomerates were found from the measurement electrode, so it can be assumed that these particles are formed inside the test cell, probably by detaching from the dendrite structures. An average charge number of approximately 7200 was also determined with the SEM-images and current measurements.

This phenomenon is also assumed to occur inside the commercial soot sensor. The dendrite structures forming on the electrode surfaces are practically essential for the operation of this sensor. This can also be confirmed from the mimic measurements, where a similar delay time of current amplification can be observed compared to sensor data. In order for the sensor to be immediately ready for use, the electrode should be coated with a substance whose morphology resembles soot agglomerate particles.

REFERENCES

Agarwal, J. K. & Sem, G. J., 1982. Continuous flow, single-particle counting condensation nucleus counter. *Journal of Aerosol Science,* 11(1), p. 343–347.

Allen, M. & Raabe, O., 1982. Re-evaluation of Millikan's oil drop data for the motion of small particles in air. *Journal of Aerosol Science,* 13(6), p. 537–547.

Balthasar, M., Mauss, F. & Wang, H., 2002. A computational study of the thermal ionization of soot particles and its effect on their growth in laminar premixed flames, *Combustion and Flame,* 129, p. 204–216.

Bilby, D., Kubinski, D. J. & Maricq, M. M., 2016. Current amplification in an electrostatic trap by soot dendrite growth and fragmentation: Application to soot sensors. *Journal of Aerosol Science,* 98(1), p. 41–58.

Broday, D. M. & Rosenzweig, R., 2011. Deposition of fractal-like soot aggregates in the human respiratory tract. *Journal of Aerosol Science,* 42, p. 372–386

Dalmaschio, C. J. & Leite, E. R., 2012. Detachment induced by Rayleigh-instability in metal oxide nanorods: Insights from TiO_2. *Cryst. Growth Des.,* 12, p. 3668–3674.

Dietrich, M., Jahn, C., Lanzerath, P. & Moos, R., 2015. Microwave-based oxidation state and soot loading determination on gasoline particulate filters with three-way catalyst coating for homogenously operated gasoline engines. *Sensors,* 15, p. 21971–21988.

Dockery, D. W., Pope III, C. A., Xu, X., Spengler, J. D., Ware, J. H., Fay, M. E., Ferris Jr., B. G. & Speizer, F. E., 1993. An association between air pollution and mortality in six U.S. cities. *N. Engl. J. Med.,* 329(24), p. 1753–1759.

Guan, B., Zhan, R., Lin, H. & Huang, Z., 2015. Review of the state-of-the-art of exhaust particulate filter technology in internal combustion engines. *Journal of Environmental Management,* 154(1), p. 225–258.

Han, C. B., Jiang, T., Zhang, C., Li, X., Zhang, C., Cao, X. & Wang, Z. L., 2015. Removal of particulate matter emissions from a vehicle using a self-powered triboelectric filter. *ACS Nano,* 9(12), p. 12552–12531.

Hinds, W. C., 1999. *Aerosol technology: Properties, behavior, and measurement of airborne particles.* 2. ed. New York: John Wiley & Sons.

Horenstein, M. N., 2004. Applied electrostatics. In: R. Bansal, *Handbook of engineering electromagnetics.* New York: Marcel Dekker, p. 53–87.

Högström, R., Karjalainen, P., Yli-Ojanperä, J., Rostedt, A., Heinonen, M., Mäkelä, J. M. & Keskinen, J., 2012. Study of the PM gas-phase filter artifact using a setup for mixing diesel-like soot and hydrocarbons, *Aerosol Science and Technology*, 46(9), 1045–1052.

John, W., 1995. Particle-surface interactions: charge transfer, energy loss, resuspension, and deagglomeration. *Atmospheric Chemistry and Physics,* 23(1), p. 2–24.

Karagulian, F., Belis, C. A., Dora, C. F. C., Prüss-Ustün, A. M., Bonjour, S., Adair-Rohani, H. & Amann, M., 2015. Contributions to cities' ambient particulate matter (PM): A systematic review of local source contributions at global level. *Atmospheric Environment,* 120(1), p. 175–483.

Keady, P. B., Quant, F. R. & Sem, G. J., 1983. Differential mobility particle sizer: A new instrument for high-resolution aerosol size distribution measurement below 1 μm. *TSI Quarterly,* 9(2), p. 3–11.

Keskinen, J., Pietarinen, K. & Lehtimäki, M., 1992. Electrical low pressure impactor. *Journal of Aerosol Science,* 23(4), p. 353–360.

Kittelson, D., 1998. Engines and nanoparticles: a review. *Journal of Aerosol Science,* 29(5/6), p. 575–588.

Knutson, E. O. & Whitby, K. T., 1975. Aerosol classification by electric mobility: Apparatus, theory, and applications. *Journal of Aerosol Science,* 11, 6(6), p. 443–451.

Kulkarni, P., Baron, P. A. & Willeke, K., 2011. *Aerosol measurement: Principles, techniques, and applications.* 3. ed. New Jersey: John Wiley & Sons.

Lanki, T. Tikkanen, J., Janka, K., Taimisto, P. & Lehtimäki, M., 2011. An electrical sensor for long-term monitoring of ultrafine particles in workplaces. *Journal of Physics: Conference Series,* 304(1).

Lelieveld, J., Evans, J. S., Fnais, M., Giannadaki, D. & Pozzer, A., 2015. The contribution of outdoor air pollution sources to premature mortality on a global scale. *Nature,* 525(7569), p. 367–371.

Lu, G., Zhu, L., Wang, P., Chen, J., Dikin, D. A., Ruoff, R. S., Yu, Y., & Ren, Z. F., 2007. Electrostatic-force-directed assembly of Ag nanocrystals onto vertically aligned carbon nanotubes. *J. Phys. Chem. C,* 111, p. 17919–17922.

Malik, A., Abdulhamid, H., Pagels, J., Rissler, J., Lindskog, M., Nilsson, P., Bjorklund, R., Jozsa, P., Visser., J., Spetz, A. & Sanati, M., 2011. A potential soot mass determination method from resistivity measurement of thermophoretically deposited soot. *Aerosol Science & Technology,* 45(2), p. 284–294.

Mansfield, M. & O'Sullivan, C., 1998. *Understanding Physics.* 1. ed. New Jersey: John Wiley & Sons.

Maricq, M. M., 2006. On the electrical charge of motor vehicle exhaust particles. *Journal of Aerosol Science,* 37(7), p. 858–874.

Mathis, U., Mohr, M. & Kaegi, R., 2005. Influence of Diesel engine combustion parameters on primary soot particle diameter. *Environmental Science and Technology,* 39(6), p. 1887–1892.

Matsusaka, S., Maruyama, H., Matsuyama, T. & Ghadiri, M., 2010. Triboelectric charging of powders: A review. *Chemical Engineering Science,* 65(22), p. 5781–5807.

Mizuno, A., 2000. Electrostatic precipitation. *IEEE Transactions on Dielectrics and Electrical Insulation,* 7(5), p. 615–624.

Ohyama, N., Nakanishi, T., & Daido, S., 2008. New concept catalyzed DPF for estimating soot loadings from pressure drop. *SAE Technical Paper.*

Olfert, J. S., Symonds, J. P. R. & Collings, N., 2007. The effective density and fractal dimension of particles emitted from a light-duty diesel engine with a diesel oxidation catalyst. *Journal of Aerosol Science,* 38(1), p. 69–82.

Onischuk, A. A., di Stasio, S., Karasev, V. V., Baklanov, A. M., Makhov, G. A., Vlasenko, A. L., Sadykova, A. R., Shipovalov, A. V. & Panfilov, V. N., 2003. Evolution of structure and charge of soot aggregates during and after formation in a propane/air diffusion flame. *Aerosol Science,* 34, p. 383–403.

Pham, H., 2006. *Springer Handbook of Engineering Statistics.* London: Springer-Verlag.

Riehle, C. & Wadenpohl, C., 1996. Electrically stimulated agglomeration on an earthed surface. *Powder Technology,* 86(1), p. 119–126.

Ristimäki, J., Virtanen, A., Marjamäki, M., Rostedt, A. & Keskinen, J., 2002. On-line measurement of size distribution and effective density of submicron aerosol particles. *Journal of Aerosol Science,* 33(11), p. 1541–1557.

Rothenbacher, S., Messerer, A. & Kasper, G., 2008. Fragmentation and bond strength of airborne diesel soot agglomerates. *Particle and Fibre Toxicology,* 5(9).

Sappok, A. Ragaller, P, Bromberg, L., Prikhodko, V., Storey, J. & Parks, J., 2016. Real-time engine and aftertreatment system control using fast response particulate filter Sensors. *SAE Technical Paper.*

Shiraiwa, M., Selzle, K. & Pöschl, U., 2012. Hazardous components and health effects of atmospheric aerosol particles: reactive oxygen species, soot, polycyclic aromatic compounds and allergenic proteins. *Free Radical Research,* 46(8), p. 927–939.

Solomon, P. A., Moyers, J. L. & Fletcher, R. A., 1983. High-volume dichotomous virtual impactor for the fractionation and collection of particles according to aerodynamic size. *Aerosol Science and Technology,* 2(4), p. 455–464.

Steppan, J., Henderson, B., Johnson, K., Yusuf Khan, M., Diller, T., Hall, M., Lourdhusamy, A., Allmendinger, K. & Matthews, R., 2011. Comparison of an on-board, real-time electronic PM sensor with laboratory instruments using a 2009 heavy-duty diesel vehicle. *SAE Technical Paper.*

Straif, K., Cohen, A. & Samet, J., 2013. *Air pollution and cancer,* Lyon: International Agency for Research on Cancer.

Virtanen, A., Ristimäki, J. & Keskinen, J., 2004. Method for measuring effective density and fractal dimension of aerosol agglomerates. *Aerosol Science and Technology,* 3(5), p. 437–446.

Wang, S. C. & Flagan, R. C., 1990. Scanning electrical mobility spectrometer. *Aerosol Science and Technology,* 13(2), p. 230–240.

Warnatz, J., Maas, U. & Dibble, R. W., 2010. *Combustion.* 4. ed. Berlin: Springer-Verlag.

APPENDIX A: DIAMETERS AND AVERAGE CHARGE NUMBERS OF PRIMARY SOOT AND CCA-PARTICLES

Table A.1 Particle diameters and average charge numbers for primary soot particles generated in the Webasto burner.

Case	E_{coll} (V/mm)	N (#)	d_{Feret} (nm)	d_{PE} (nm)	n_{avg}
B1	70	467	105	80	3.7
B2	70	157	95	71	3.3
B3	70	1221	94	71	29.7
C4	70	681	87	62	3.0
C5	70	736	80	62	19.3

Table A.2 Particle diameters and average charge numbers for CCA-particles.

Case	E_{coll} (V/mm)	N (#)	d_{Feret} (µm)	d_{PE} (µm)	n_{avg}
13	500	496	5.7	3.8	8300
15	500	358	3.1	2.2	6100
A3	500	1007	8.0	5.4	10000
A4	350	596	6.2	4.5	8800
A5	200	374	4.2	3.4	8800
C1	500	1141	9.0	6.0	5500
C2	300	539	13.3	7.8	6000
C3	100	675	5.6	4.2	4000
D1	500	147	7.0	5.1	4900

APPENDIX B: MICROSCOPE IMAGES FROM THREE-ELECTRODE MIMIC CELL MEASUREMENTS

PRIMARY SOOT PARTICLES

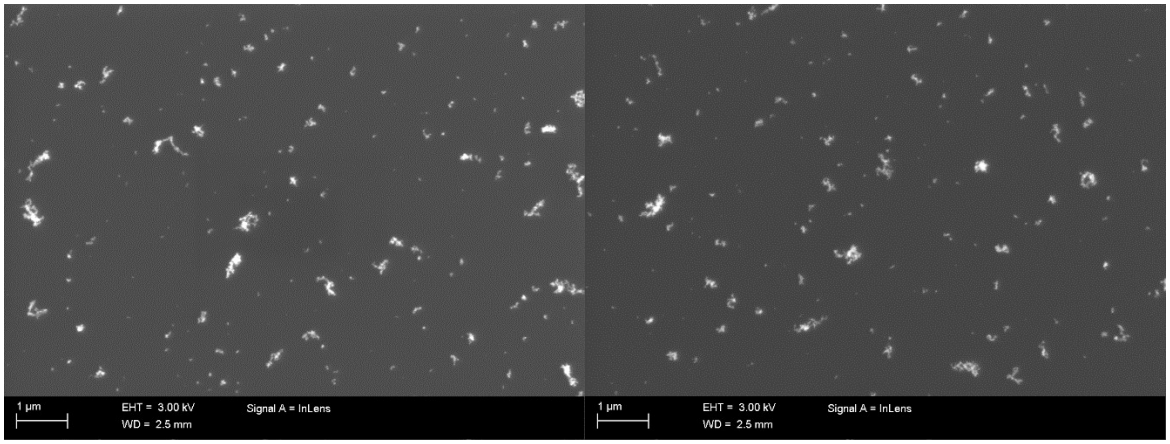

Case B1. Charge per frame: 0.14 fC

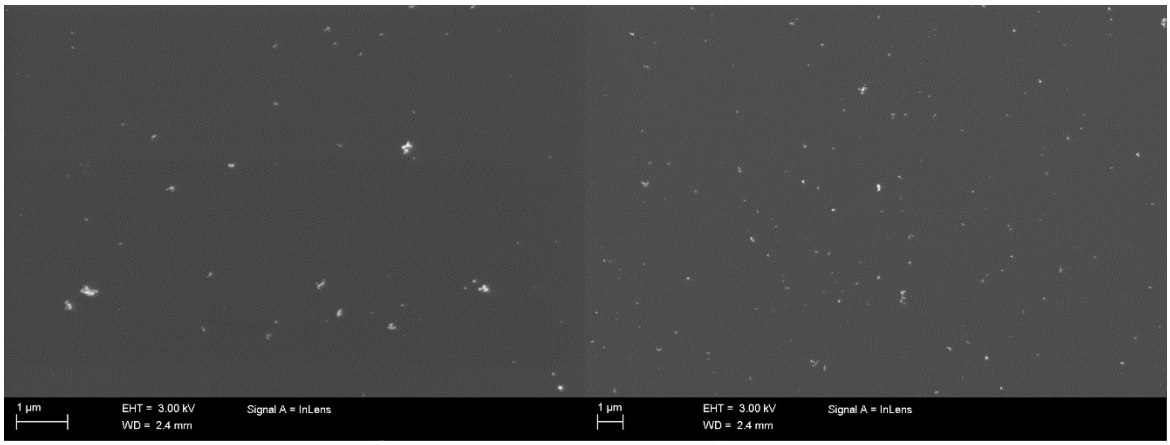

Case B2. Charge per frame: 0.042 fC

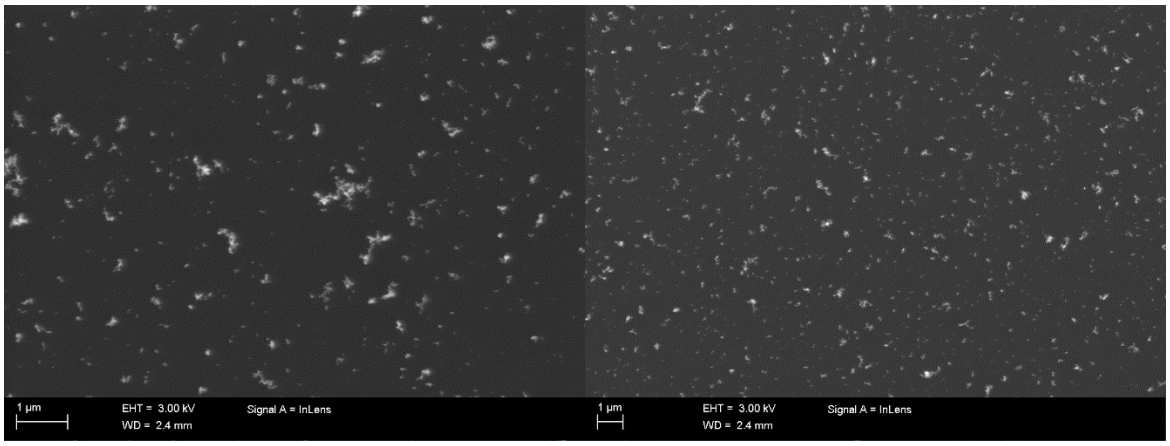

Case B3. Charge per frame: 2.9 fC

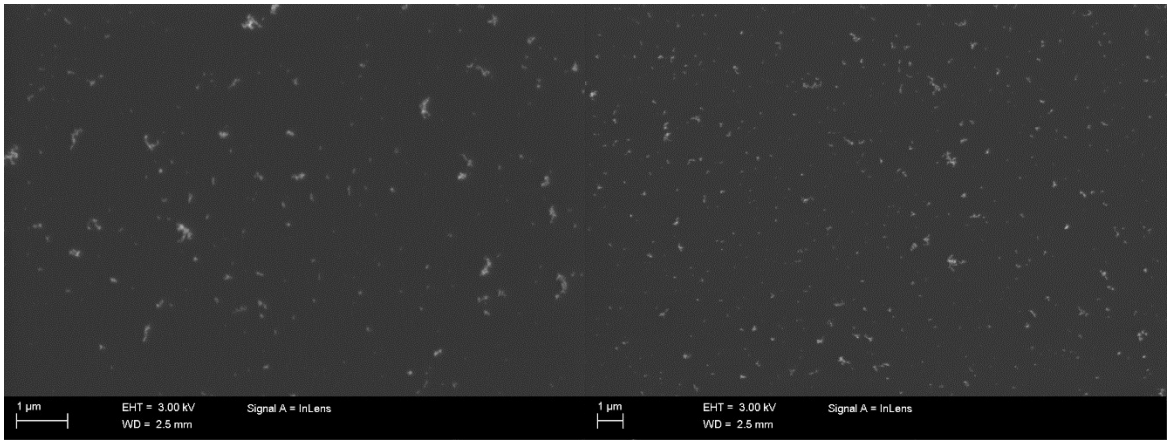

Case C4. Charge per frame: 0.16 fC

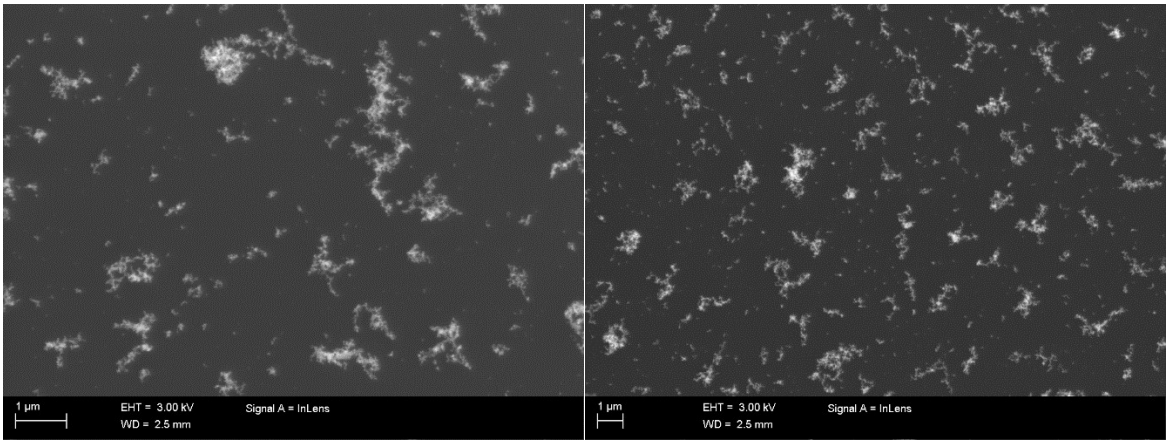

Case C5. Charge per frame: 1.1 fC

CCA-PARTICLES

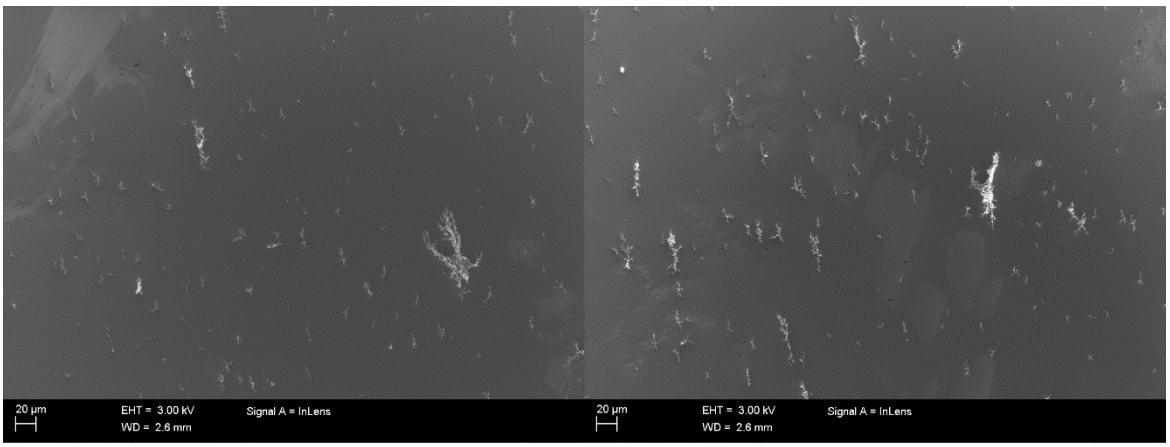

Case 13. Charge per frame: 0.33 pC

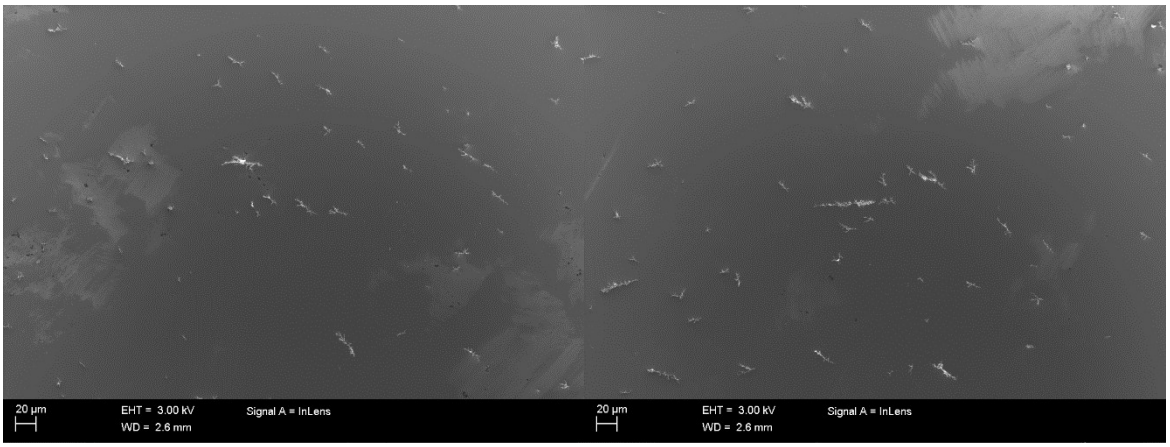

Case 15. Charge per frame: 0.17 pC

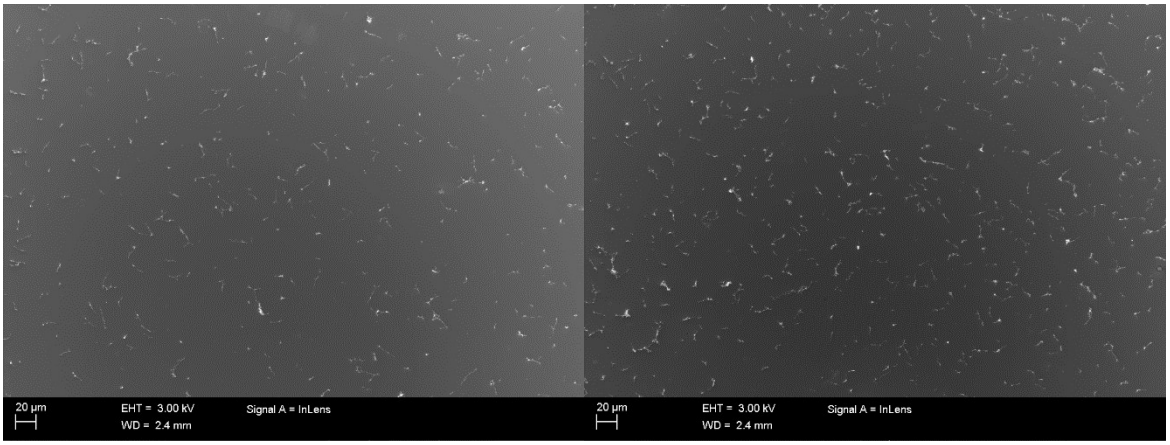

Case A3. Charge per frame: 0.80 pC

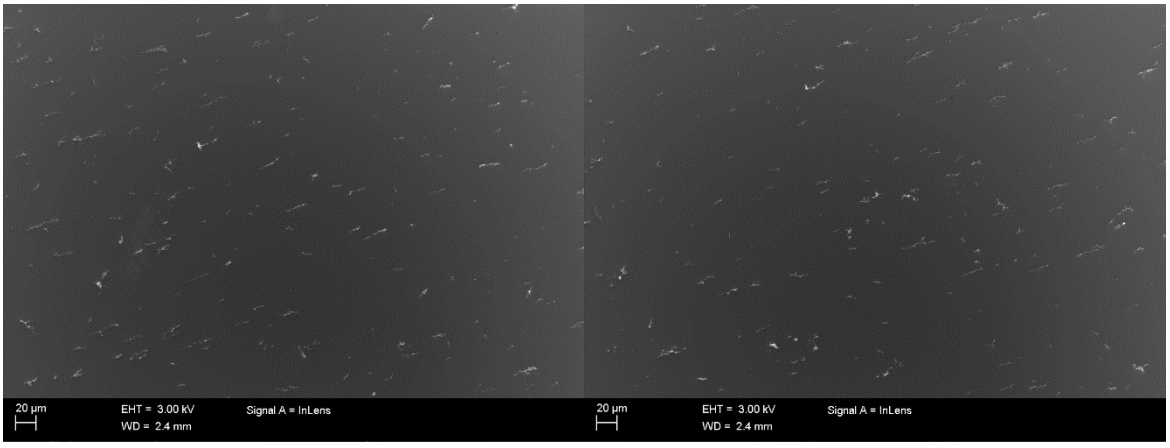

Case A4. Charge per frame: 0.42 pC

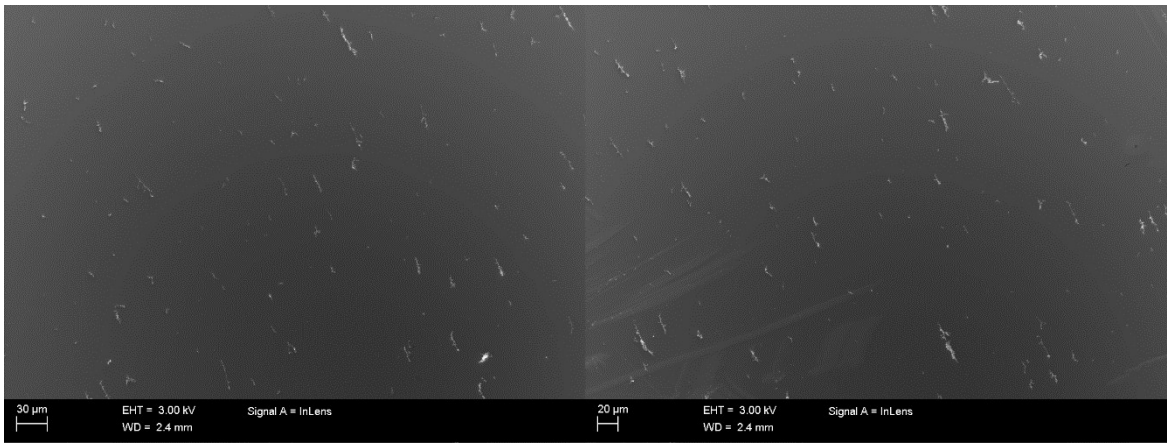

Case A5. Charge per frame: 0.33 pC

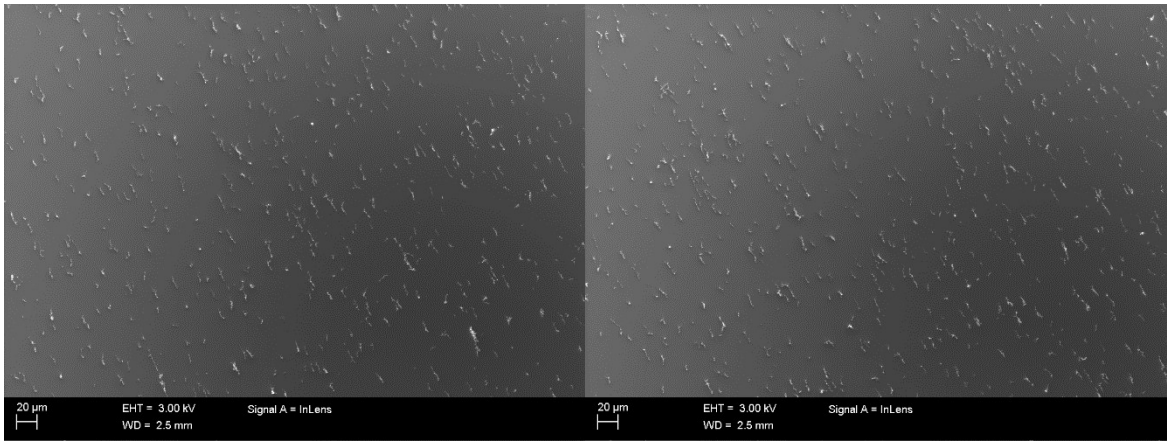

Case C1. Charge per frame: 0.50 pC

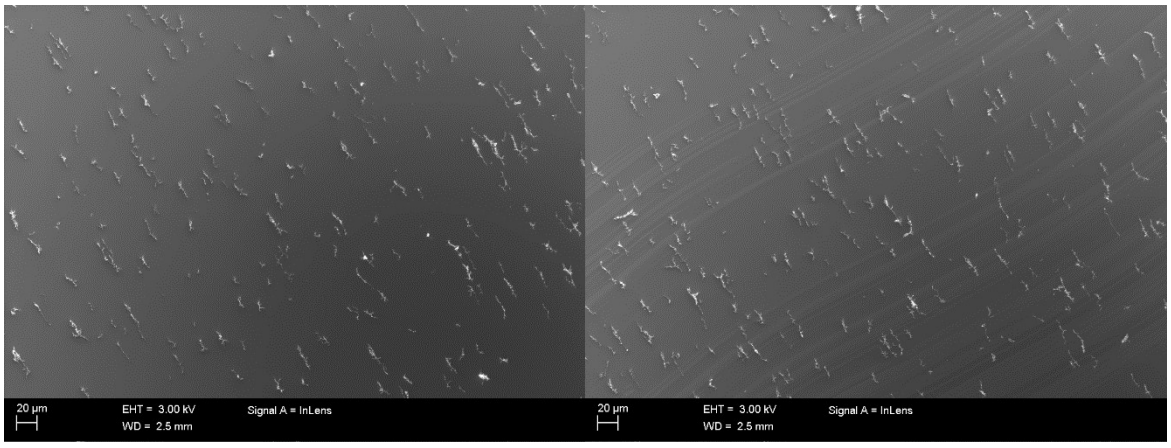

Case C2. Charge per frame: 0.26 pC

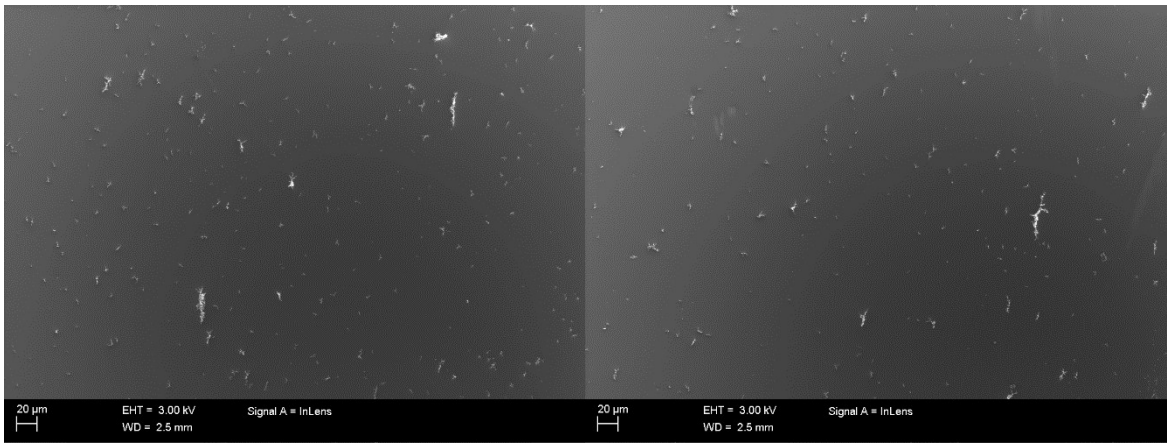

Case C3. Charge per frame: 0.22 pC

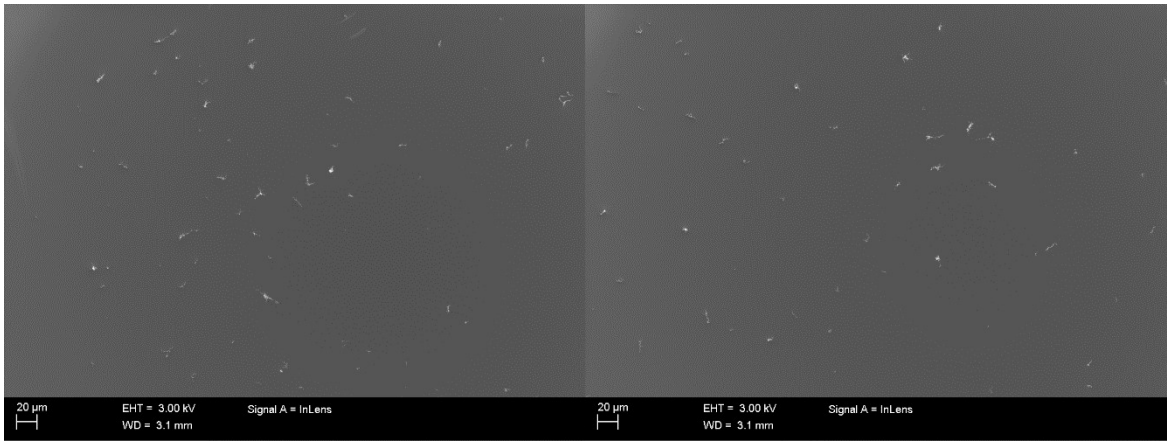

Case D1. Charge per frame: 0.058 pC